Applied Surface Science 520 (2020) 146344

Contents lists available at ScienceDirect

Applied Surface Science

journal homepage: www.elsevier.com/locate/apsusc

Microwave-assisted synthesis of a TiO_2-CuO heterojunction with enhanced photocatalytic activity against tetracycline

Adam Kubiak[a], Zuzanna Bielan[b], Marta Kubacka[a], Elżbieta Gabała[c], Agnieszka Zgoła-Grześkowiak[d], Marcin Janczarek[a], Maciej Zalas[e], Anna Zielińska-Jurek[b], Katarzyna Siwińska-Ciesielczyk[a], Teofil Jesionowski[a,*]

[a] Poznan University of Technology, Faculty of Chemical Technology, Institute of Chemical Technology and Engineering, Berdychowo 4, PL-60965 Poznan, Poland
[b] Gdansk University of Technology, Faculty of Chemistry, Department of Chemical Technology, Narutowicza 11/12, PL-80233 Gdansk, Poland
[c] National Research Institute, Institute of Plant Protection, Węgorka 20, PL-60318 Poznan, Poland
[d] Poznan University of Technology, Faculty of Chemical Technology, Institute of Chemistry and Electrochemistry, Berdychowo 4, PL-60965 Poznan, Poland
[e] Adam Mickiewicz University, Poznan, Faculty of Chemistry, Uniwersytetu Poznańskiego 8, PL-61614 Poznan, Poland

ARTICLE INFO

Keywords:
Titania
Copper(II) oxide
Microwave-assisted synthesis
Heterojunction
Z-scheme
Photocatalysis

ABSTRACT

A microwave method was used for the synthesis of TiO_2-CuO oxide systems. A detailed investigation was made of the effect of the molar ratio of components (TiO_2:CuO = 9:1, 7:3, 5:5, 3:7, 1:9) on the crystalline structure and morphology. Transmission electron microscopy (TEM) confirmed the presence of octahedral and rod-shaped titania particles and sheet copper(II) oxide particles; moreover, HRTEM analysis indicated the presence of a heterojunction between TiO_2 and CuO. The synthesized materials were analyzed by X-ray diffraction (XRD) and Raman spectroscopy, and two crystalline forms (anatase and monoclinic CuO) were detected. The key element of the work was to determine the photocatalytic activity of the obtained binary oxide systems in the degradation of tetracycline. Photo-oxidation tests proved that the binary oxide materials (especially the (9)TiO_2-(1)CuO and (7)TiO_2-(3)CuO samples) demonstrate high photocatalytic activity in the decomposition of tetracycline (95% after 90 min irradiation) compared with the reference titania samples. Furthermore, a Z-scheme heterojunction photocatalytic process mechanism was proposed. Another important part of the work was the determination of tetracycline photodegradation products using the HPLC/MS technique.

1. Introduction

Pharmaceuticals and other chemicals used in everyday life have recently become a new source of environmental micro-pollutants [1,2]. Non-steroidal, anti-inflammatory drugs, hormones and antibiotics contained in wastewater pose a potential threat to the aquatic ecosystem, as they may reach underwater media as a result of sewage discharge from treatment plants [3,4], and to the terrestrial ecosystem, if the treated sediment is used as a fertilizer [5]. In addition, it is believed that pharmacological agents in wastewater residues contribute to changes in the human body, since even very small amounts of antibiotics in the daily diet lead to the production of resistant strains of bacteria and may cause allergies [6,7]. The occurrence and fate of pharmaceuticals and antibiotics at wastewater treatment plants have been the subject of many scientific studies [8-10]. Tetracycline is the world's second most common antibiotic in terms of production and human use [3,11]. It has a wide range of applications, for example in preventing infections caused by microorganisms in humans and animals [12]. It is currently estimated that about 25–75% of the tetracycline antibiotics ingested by the population are excreted, and as a result are discharged into urban wastewater [13]. These compounds have been detected in water, soil, sewage and activated sludge [14,15] in concentrations ranging from 2 ng/L up to 50 μg/L [16,17]. Scientists have proposed various methods of removing antibiotics from sewage sludge, including adsorption [6,7], ozone treatment [18] and photocatalysis [3]. In comparison with other techniques, photocatalysis has been identified as a green and effective technique for tetracycline degradation from sewage sludge [3].

In the existing literature, one of the most commonly reported photocatalytic materials is titanium dioxide (for which the number of publications in the Scopus database is 11 861 in 2019 alone). Titania is one of the most popular semiconductor photocatalysts, characterized by chemical and thermal resistance, non-toxicity, resistance to corrosion and relatively low price [19,20]. This material is finding a growing

* Corresponding author.
E-mail address: teofil.jesionowski@put.poznan.pl (T. Jesionowski).

https://doi.org/10.1016/j.apsusc.2020.146344
Received 1 January 2020; Received in revised form 2 April 2020; Accepted 14 April 2020
Available online 18 April 2020

range of photocatalytic applications, with research currently focused on such areas as elimination of environmental pollution [21], solar cells [22] and self-cleaning surfaces [23]. Despite the above-mentioned advantages, a significant limitation is the reduction in the photocatalytic activity of titanium dioxide caused by the recombination of electron-hole pairs, which is characteristic for all semiconductor materials [24]. In recent years, scientists have proposed various methods to improve the photocatalytic efficiency of titanium dioxide in the UV light region, such as surface modification [25], doping of TiO_2 [26] or semiconductor combination [27]. Among the many techniques, it is beneficial to consider in more detail the method of joining TiO_2 (which is an n-type semiconductor with wide band gap) with semiconductor materials, for example with p-type semiconductors (with narrow band gap) [28]. This operation results in a heterojunction.

A heterojunction is a medium made of two different types of material with different energy gap values on both sides of the connector. An interesting structure based on a heterojunction is an oxide system which consists of TiO_2 and CuO semiconductors. Copper(II) oxide, due to its narrow-gap (1.2–1.5 eV) semiconductor properties, is widely used, for example in the photocatalytic degradation of organic pollutants, as an antimicrobial agent or as a catalytic material [29]. It is also a promising material for the production of solar cells, due to its high absorption of solar radiation, low thermal emission and relatively good electrical properties [30]. Many reports have been published on innovative applications of TiO_2 modified with copper(II) oxide in photocatalysis [31,32]. The formation of a heterojunction of type II is caused by the excitation of an electron from the valence band to the conductive band of copper(II) oxide and its transfer the conductive band to titania [33,34]. The combination of titanium dioxide and copper(II) oxide has a number of advantages, since the TiO_2-CuO oxide system has significantly better optical and photocatalytic properties than TiO_2 or CuO alone [35,36].

The key objective of this work was a microwave synthesis of a novel TiO_2-CuO oxide materials, which will be tested as photoactive agent in the degradation of a model organic pollutant – tetracycline. It is expected that proposed synthesis method will allow to form stable heterojunction, which should facilitate the electron-hole separation and enhance the catalytic activity of synthesized materials. Furthermore, it was shown that the synthesized materials contain the well-defined crystalline structures of both anatase and monoclinic CuO, and this enabled high efficiency to be obtained in the photocatalytic process. In addition, a photocatalytic reaction mechanism based on a Z-scheme heterojunction was proposed.

2. Experimental

2.1. Materials

Titanium(IV) chloride (97%), commercial titanium dioxide P25 (Aeroxide® P25), copper(II) acetate monohydrate (99.5%), poly(ethylene glycol) (PEG, M_n = 8000) and sodium hydroxide (99.5%) were purchased from Sigma-Aldrich (USA). LC/MS-grade acetonitrile and formic acid were also from Sigma-Aldrich (USA). HPLC-grade water was prepared by reverse osmosis in a Demiwa system from Watek (Ledec nad Sazavou, Czech Republic) followed by double distillation from a quartz apparatus. All reagents were of analytical grade and used without any further purification. The water used in all experiments was deionized.

2.2. Preparation of TiO_2-CuO photocatalysts

The preparation of the TiO_2-CuO oxide system consisted of two stages. First, a 10% aqueous solution of $TiCl_4$ was prepared, and 100 mL of 10% titanium(IV) chloride was placed in a reactor on a magnetic stirrer (IKA Werke GmbH, Germany). Next, at a dosing rate of 5 mL/min, a 5 M solution of sodium hydroxide was added until the pH reached 10. The resulting reaction mixture was then transferred to a SP-D 80 microwave reactor (CEM, USA) and heated at 200 °C for 10 min at a power of 300 W. The obtained titanium dioxide was filtered, washed three times with deionized water, and dried at 105 °C for 12 h. Subsequently, the synthesis of photocatalytic TiO_2-CuO oxide systems was carried out. In 25 mL of a 5% aqueous solution of copper(II) acetate, 2 g of poly(ethylene glycol) (PEG) was added. The PEG was used as a modifier to improve the connection between TiO_2 and CuO. The obtained solution was then placed in a reactor on a magnetic stirrer, and 1 M sodium hydroxide solution was added until the pH reached 12. The titania prepared in the first step was sonicated for 10 min in water (SONIC-3 ultrasonic cleaner, POLSONIC, Poland), and was then added to the reaction mixture and stirred for 30 min. Finally, the obtained mixture was subjected to microwave treatment at 150 °C for 10 min at a power of 300 W (SP-D 80, CEM). The synthesized oxide systems were filtered and washed three times with deionized water and dried at 70 °C for 7 h. Materials were obtained at the molar ratios TiO_2:CuO = 10:0, 9:1, 7:3, 5:5, 3:7, 1:9, 0:10, being respectively labeled TiO_2, (9)TiO_2-(1)CuO, (7)TiO_2-(3)CuO, (5)TiO_2-(5)CuO, (3)TiO_2-(7)CuO, (1)TiO_2-(9)CuO, and CuO.

2.3. Characterization of synthesized materials

The crystalline phases of the synthesized oxide systems were determined by X-ray diffraction analysis (XRD) and Raman spectroscopy. XRD analysis was performed with a D8 Advance diffractometer (Bruker, Germany) operating with Cu Kα radiation (α = 1.5418 Å), Ni filtered. The patterns were obtained in step-scanning mode (Δ2θ = 0.05°) over an angular range of 20–80°. The crystallite size of photocatalysts in the direction vertical to the corresponding lattice plane was determined using the Scherrer equation [37,38], based on the corrected full width at half maximum (FWHM) of the XRD peak and angle of diffraction. Raman spectroscopy was performed using a Bruker Bravo analyzer (Bruker, Germany). To obtain the spectrum, the tested material was put on a glass slide and placed in a measuring cell. Measurements were made in the range 800–300 cm^{-1}.

The light-absorption properties of all synthesized oxide materials were measured using diffuse reflectance spectroscopy (DRS) in the range of 200–800 nm. The band gap energy of obtained samples was calculated from $(F(R)\cdot E)^{0.5}$ against E graph, where E is photon energy and F(R) is Kubelka-Munk function, proportional to the radiation's absorption. The measurements were carried out using Thermo Scientific Evolution 220 spectrophotometer (Waltham, USA) equipped with a PIN-757 integrating sphere, using $BaSO_4$ as a reference.

To determine the morphology of the obtained oxide materials, transmission electron microscopy was performed using a Jeol 1200 EX II instrument (Jeol, Japan). Furthermore, high-resolution transmission electron microscopy (HRTEM) measurements were made with a Hitachi HT7700 microscope (Hitachi, Japan), operating at 100 kV.

The X-ray Photoelectron Spectroscopy (XPS) experiments were recorded on Specs UHV spectrometer (SPECS, Germany) with a charge neutralizer. The C 1s peak at 284.8 eV was used as a reference to rectify the binding energies.

An ASAP 2020 physisorption analyzer (Micromeritics Instrument Co., USA) was used to determine the parameters of the porous structure of the TiO_2-CuO oxide systems, including Brunauer–Emmett–Teller (BET) surface area, pore volume and pore size, using low-temperature N_2 sorption. Before measurement, the analyzed materials were degassed at 120 °C for 4 h. The surface area was determined by the multipoint BET method using adsorption data for relative pressure (p/p_o) in the range 0.05–0.30.

Thermogravimetric analysis was performed using a Jupiter STA 449 F3 instrument (Netzsch GmbH, Germany). Measurements were made under flowing nitrogen at a heating rate of 10 °C/min in a temperature range of 30–1000 °C.

2.4. Photocatalytic test

To determine the photocatalytic activity of the obtained TiO_2-CuO oxide systems, photodegradation of a model organic pollutant – tetracycline – was carried out in a UV laboratory reactor (UV-RS2, Heraeus, Germany) made of quartz glass. The reactor is equipped with a 150 W medium-pressure mercury lamp as a UV light source, surrounded by a water-cooling quartz jacket. Initially, 100 mL of the model organic impurity (tetracycline 50 mg/L) and an appropriate quantity (0.1 g) of the photocatalyst were introduced into the reactor. The resulting suspension was homogenized using an R05 IKAMAG magnetic stirrer (IKA Werke GmbH, Germany), in darkness, for 30 min to establish adsorption/desorption equilibrium. After this time, the lamp was switched on and the reaction mixture was irradiated. To investigate the efficiency of photodegradation, samples were taken at specific time intervals (every 10 min up to 1.5 h), centrifuged (5810R centrifuge, Eppendorf, Germany), and finally analyzed using a UV–Vis spectrophotometer (V-750, Jasco) in the wavelength range 200–700 nm, using water as a reference. The maximum absorbance for the test samples at wavenumber 357 nm was observed. The concentration of adsorbed or degraded tetracycline was read off from the calibration curve [Tetracycline] = 0.0331*Abs. The photocatalytic activity of the TiO_2-CuO oxide systems was determined by calculating the yield of dye degradation (W), using the formula:

$$W(\%) = \left(1 - \frac{C_t}{C_0}\right) \cdot 100\%$$

where C_0 and C_t are the concentrations of the dye prior to and after irradiation.

In order to determine the mineralization efficiency the total organic carbon (TOC) were carried out. The measurements were conducted using TOC-L analyzer (Shimadzu, Japan).

2.5. Chromatographic measurements

Identification of degradation products was carried out using an UltiMate 3000 HPLC instrument (Dionex, Sunnyvale, CA, USA) coupled with a 4000 QTRAP mass spectrometer (AB-Sciex, Foster City, CA, USA). A Kinetex Evo C18 column (150 mm × 2.1 mm; I.D. 2.6 μm) from Phenomenex (Torrance, CA, USA) maintained at 35 °C was used in the study. The sample injection volume was 5 μL. The mobile phase consisted of 0.1% formic acid in water and acetonitrile (ACN) at a flow rate of 0.3 mL/min using the following gradient: 0 min 10% ACN, 1 min 10% ACN, 3 min 40% ACN, 6 min 85% ACN. The electrospray ion source (ESI) operated in positive mode. Nitrogen was used in both the source and the mass spectrometer. The following parameters of the source and mass spectrometer were used: curtain gas pressure 10 psi, nebulization gas pressure 45 psi, auxiliary gas pressure 45 psi, source temperature 450 °C, ESI voltage 4500 V, declustering potential 45 V. Chromatograms were collected in enhanced mass spectra mode in the scan range m/z = 50–600. Selected ions were fragmented in enhanced product ion mode.

3. Results and discussion

3.1. Crystalline structure

To determine the crystalline structure of the obtained TiO_2-CuO oxide systems, the techniques of X-ray diffraction and Raman spectroscopy were applied. Fig. 1a shows the XRD patterns of the synthesized TiO_2-CuO oxide systems and reference samples.

For reference samples of titanium dioxide and copper(II) oxide obtained by the microwave method, characteristic bands for the structure of anatase (JCPDS No. 21-1272) and monoclinic CuO (JCPDS 41-0254) respectively were observed. It was found that the crystalline planes (1 0 1), (0 0 4), (2 0 0), (1 0 5), (2 0 4), (1 1 6), (2 2 0), (2 1 5) occur in the TiO_2 sample, while the planes (1 1 0), (0 0 2), (1 1 1), (2 0 2), (1 1 3), (0 2 2), (3 1 1) were observed for the reference CuO. It should be noted that there is not much previous work on the synthesis of titania using fast and short microwave treatment. Dar et al. [39] described the synthesis of titania using a microwave method; however, a thiobenzoate complex of titanium was used for the synthesis, which may have affected the size of the crystallites (5–7 nm) and contributed to the lower crystallinity of the material. Corradi et al. [40] used microwave treatment to obtain titanium dioxide with a rutile crystalline structure. In turn, Falk et al. [41] obtained an anatase crystalline structure, although the synthesized material was additionally calcined. The most similar titania material to that received in this work, was obtained by Wang et al. [42], who used TiO_2 nanoparticles in dye-sensitized solar cells. As with titanium dioxide, the synthesis of copper (II) oxide using the microwave method is not widely described in the scientific literature. Volanti et al. [43] developed a synthesis of copper (II) oxide using a one-step microwave method. They obtained a material with good crystallinity, but with a much longer microwave treatment time (1 h) compared with the materials described in this work. Similar crystalline structures of monoclinic CuO have also been described by Yang et al. [44] and Qiu et al. [45]. However, attention should be paid to factors such as the choice of precursors and the parameters of microwave treatment, which can have an impact on the physicochemical properties. The two-stage microwave synthesis proposed in this work led to well-formed crystalline structures of anatase and monoclinic CuO for all of the resulting TiO_2-CuO oxide systems. Moreover, for the all analyzed oxide samples the characteristic reflections associated with metallic Cu and Cu_2O are absent. We also observed that increasing the molar contribution of CuO leads to the formation of more intensive reflections characteristic for this structure, and the reflection corresponding to anatase significantly decreased. Table 1 shows the crystallite sizes of the synthesized oxide materials. The crystallite size was determined for the crystalline plane (1 0 1) of anatase and (1 1 1) of monoclinic CuO. The determined crystallite size, based on the Scherrer equation [37,38], indicates that the microwave synthesis of TiO_2-CuO oxide systems improved the crystallinity of anatase, as manifested in an increase in the size of crystallites. The (9)TiO_2-(1)CuO oxide system is characterized by average size of crystallites of 19.8 nm for anatase compared with 12.7 nm for the reference titania. For the materials obtained at the molar ratios TiO_2:CuO = 7:3; 5:5 and 3:7, a similar crystallite size was observed for the crystalline structures of anatase and monoclinic CuO. However, for the (1)TiO_2-(9)CuO system, the crystallite size (17.2 nm) of monoclinic copper(II) oxide was similar to that of the CuO reference sample (17.5 nm). Obtained results proved that crystallite sizes of anatase decrease with increasing content of CuO in binary oxide materials. This fact probably is related to crystallites growth competition between these two oxides. The presence of CuO likely hinder the growth of TiO_2 crystallites. We also observed that with an increasing amount of copper precursor in the synthesis of mixed oxide materials size of CuO crystallites also increased. Based on the XRD analysis results it was also possible to evaluate the relative content of anatase and monoclinic CuO phases in synthesized materials. For example, sample (9)TiO_2-(1)CuO is composed with 87.8% of anatase and 12.2% of monoclinic CuO, sample (5)TiO_2-(5)CuO contains 52.1% and 47.9% and sample (1)TiO_2-(9)CuO – 12.5% and 87.5% of anatase and CuO (see Table 1), respectively. The relative percentage content of monoclinic CuO increase together with increasing amount of copper precursor.

To confirm the presence of well-formed crystalline structures, Raman spectroscopy was used (Fig. 1b). For the reference titania sample, characteristic bands with the Raman shifts 398 cm^{-1} (B_{1g}), 516 cm^{-1} (A_{1g}/B_{1g}) and 637 cm^{-1} (E_g) were observed. Moreover, for the CuO sample, bands were found at the Raman shifts 330 cm^{-1} (B_g) and 616 cm^{-1} (B_g). The Raman spectra obtained for the reference materials are consistent with the available scientific literature [46,47].

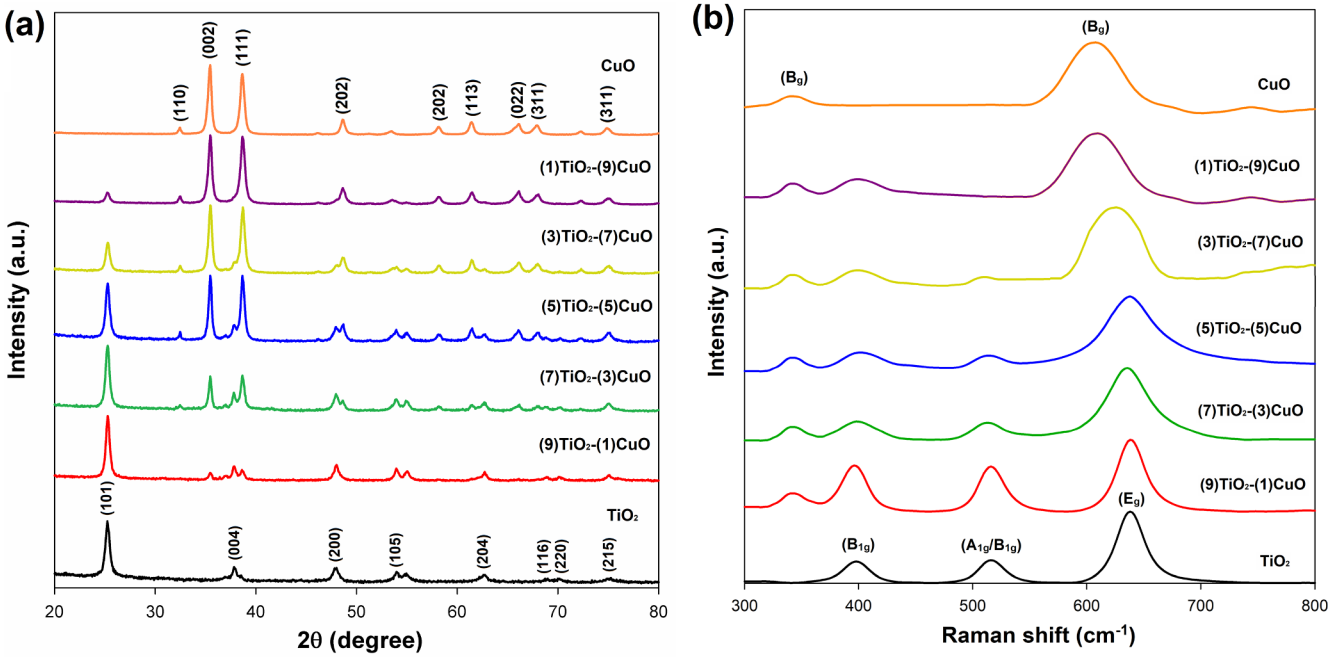

Fig. 1. XRD patterns (a) and Raman spectra (b) for TiO_2, TiO_2-CuO oxide systems and CuO.

For all of the obtained TiO_2-CuO oxide systems, crystalline structures are observed for both anatase and monoclinic CuO. For the materials synthesized with the molar ratios TiO_2:CuO = 7:3, 5:5 and 3:7 a band shift in the range 500–700 cm^{-1} was observed, associated with the occurrence of bands derived from anatase and monoclinic copper(II) oxide at almost the same Raman shift. Raman spectroscopy confirmed the coexistence of two well-formed crystalline structures (anatase and monoclinic CuO) in the oxide systems synthesized via a two-stage microwave method. The results obtained from Raman spectroscopy were found to be consistent with the previously described X-ray diffraction analysis.

There is a small number of existing scientific reports on the synthesis of TiO_2-CuO oxide systems. In works such as those of Lee et al. [31,32] and Zhu et al. [48] the electrospinning method was used to synthesize the materials. This method is significantly different from the microwave treatment used in the present work, and this was a decisive factor in the differences in crystalline structure. Moreover, the use of a facile reduction/deposition technique [49] and a hydrothermal method [50] again did not lead to high-crystalline monoclinic CuO structures. The fast two-stage microwave synthesis made it possible to obtain well-formed crystalline structures of both anatase and monoclinic CuO, which has not been observed in previous work.

3.2. Diffuse reflectance spectroscopy

In order to determine the band gap energies of synthesized TiO_2-CuO oxide system, the diffuse reflectance spectroscopy (DRS) analysis were carried out. The results of DSR analysis are shown in Table 1.

The energies of band gap of synthesized titania and copper(II) oxide are 3.2 eV and 1.7 eV, respectively. The obtained results are similar to others scientific reports [33-36]. For the TiO_2-CuO oxide systems the change of band gap was observed. With increasing content of copper(II) oxide in analyzed samples the band gap decreases from 2.9 to 1.8 for TiO_2-CuO materials. It means that addition of CuO has a significant effect on the optical absorption of TiO_2-CuO photocatalysts. Obtained results indicate that binary oxide materials probably will be characterized with better photocatalytic activity compared with TiO_2. Morover, the presented results are with agreement with research by Etape et al. [51] and Cahino et al. [52] who synthesized materials based on copper(II) oxide.

3.3. Morphology

The morphology of the obtained oxide materials was evaluated using a transmission electron microscope (Fig. 2).

For the reference samples of both titanium dioxide and copper(II) oxide, the particle shapes characteristic of the respective crystalline structures – anatase and monoclinic CuO – were observed. These were

Table 1
Size of crystallites, phase composition and band gap energies of synthesized oxide materials.

Sample	Crystallites size (nm)		Phase composition* (%)		Band gap energy (eV)
	Anatase	Monoclinic CuO	Anatase	Monoclinic CuO	
TiO_2	12.7	–	100	–	3.2
(9)TiO_2-(1)CuO	19.8	11.4	87.8	12.2	2.9
(7)TiO_2-(3)CuO	16.5	15.8	67.1	32.9	2.8
(5)TiO_2-(5)CuO	16.2	16.4	52.1	47.9	2.2
(3)TiO_2-(7)CuO	16.1	17.3	31.4	68.6	2.0
(1)TiO_2-(9)CuO	14.1	17.4	12.5	87.5	1.8
CuO	–	17.5	–	100	1.7

* Without consideration of amorphous phase.

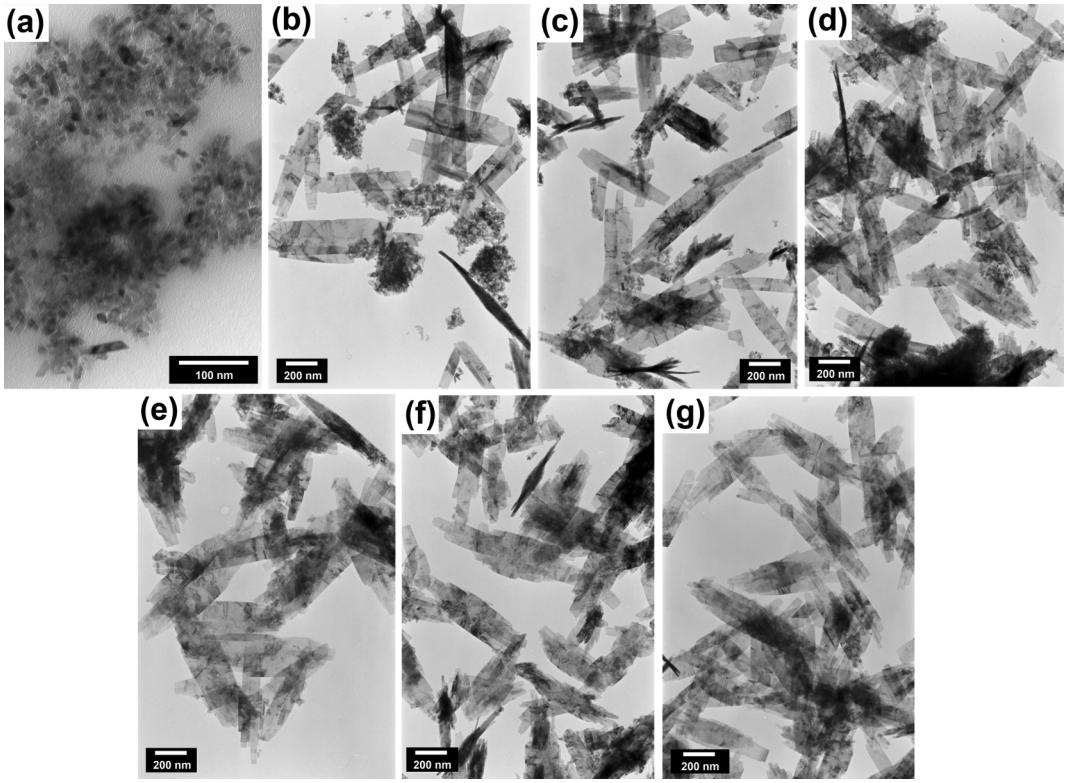

Fig. 2. TEM images for (a) titania, oxide materials obtained at TiO_2:CuO molar ratios of (b) 9:1; (c) 7:3; (d) 5:5; (e) 3:7; (f) 1:9 and (g) copper(II) oxide.

octahedral and nanorod-shaped particles in the case of TiO_2, and particles in the form of nanosheets for CuO. The octahedral TiO_2 particles had sizes of less than 25 nm, while the rods were of varying length, typically not greater than 50 nm. The CuO nanosheets were approximately 200 nm wide and 1000 nm long. In the obtained TiO_2-CuO oxide systems, both copper(II) oxide nanosheets and titania nanoparticle aggregates can be observed. Moreover, for all analyzed TiO_2-CuO oxide systems the heterogeneous particle sizes were observed. The particles of titania created the aggregates with diameter about 200 nm, but it should be noted that the above-mentioned particles are on the copper (II) oxide sheets. What's more the size of CuO sheets is not homogenous, because we can observed the particles with length 100 nm and bigger. Therefore it should be indicated, that the size of copper(II) oxide sheets is in the range – 200–800 nm (length) and 100–200 nm (width).

The occurrence of this type of morphology may allow the formation of a heterojunction, which may affect many functional properties of the resulting materials. To confirm the existence of a surface junction between titanium dioxide and copper(II) oxide, HRTEM analysis (Fig. 3) with EDS mapping (Figs. 4 and 5) was performed for selected materials ((7)TiO_2-(3)CuO and (3)TiO_2-(7)CuO samples).

The analyzed oxide materials were found to have crystallographic spacing characteristic for plane (1 0 1) of anatase (0.35 nm) and (1 1 1) of monoclinic CuO (0.24 nm). The HRTEM results are consistent with those of XRD and Raman analysis, which also indicate the high crystallinity of the obtained materials. Attention was also paid to the crossing of lattice fringes of titania and copper(II) oxide. The existence of such connections has been described in the scientific literature as a heterojunction [50]. Because titania is an n-type semiconductor and copper(II) oxide is a p-type semiconductor, the formation of a heterojunction is possible, and this is extremely important in producing binary oxide materials with superior properties to those of the reference samples. Moreover, the similar crystalline lattice distances obtained for the materials (7)TiO_2-(3)CuO and (3)TiO_2-(7)CuO indicate that irrespective of the molar ratio, titania was applied effectively to the CuO sheet structure. This was enabled by the use of poly(ethylene glycol) as a surfactant. To determine the distribution of TiO_2 on the CuO surface, EDS mapping was performed. Figs. 4 and 5 present the results of EDS analysis for the materials (7)TiO_2-(3)CuO and (3)TiO_2-(7)CuO, respectively.

Based on the results of EDS – both mapping and point analysis – for the analyzed oxide systems, it was found that titania is present on the sheets of copper(II) oxide. However, it should be noted that the distribution of titanium dioxide particles is not homogeneous. The obtaining of a titania coating on the copper(II) oxide was made possible by the use of PEG. Many reports, such as those of Yu et al. [53] and Rahim et al. [54], indicate that the use of non-ionic surfactants makes it possible to synthesize materials with a defined morphology. Furthermore, in the combination of CuO with TiO_2 it is important in order to obtain a surface junction, and in particular a heterojunction.

When the results of the morphological analysis are compared with those in the existing literature, the novelty of the present work should be borne in mind. To date, such materials have been obtained mainly by the electrospinning method, as reported in such works as those of Lee et al. [31,32] and Zhu et al. [48]. Note should be taken of two papers on TiO_2-CuO heterojunctions, by Nagaraju et al. [50] and Shi et al. [49], but these do not describe heterojunctions for materials obtained by microwave treatment. There are also clear differences in morphology between the materials described in this work and the previous systems with heterojunctions [49,50]. Therefore, in our view, the microwave method can be indicated as an effective method for the synthesis of heterojunction TiO_2-CuO oxide systems.

3.4. X-ray Photoelectron spectroscopy

The analysis of chemical states of the elemental components of prepared materials has been made using the XPS technique. As it was expected three elements that were incorporated into the synthesis procedure, i.e., Ti, O, and Cu may be observed in the spectra of all presented materials (except Ti in CuO spectrum and Cu in TiO_2 spectrum) and the selected high-resolution XPS spectra of specific regions,

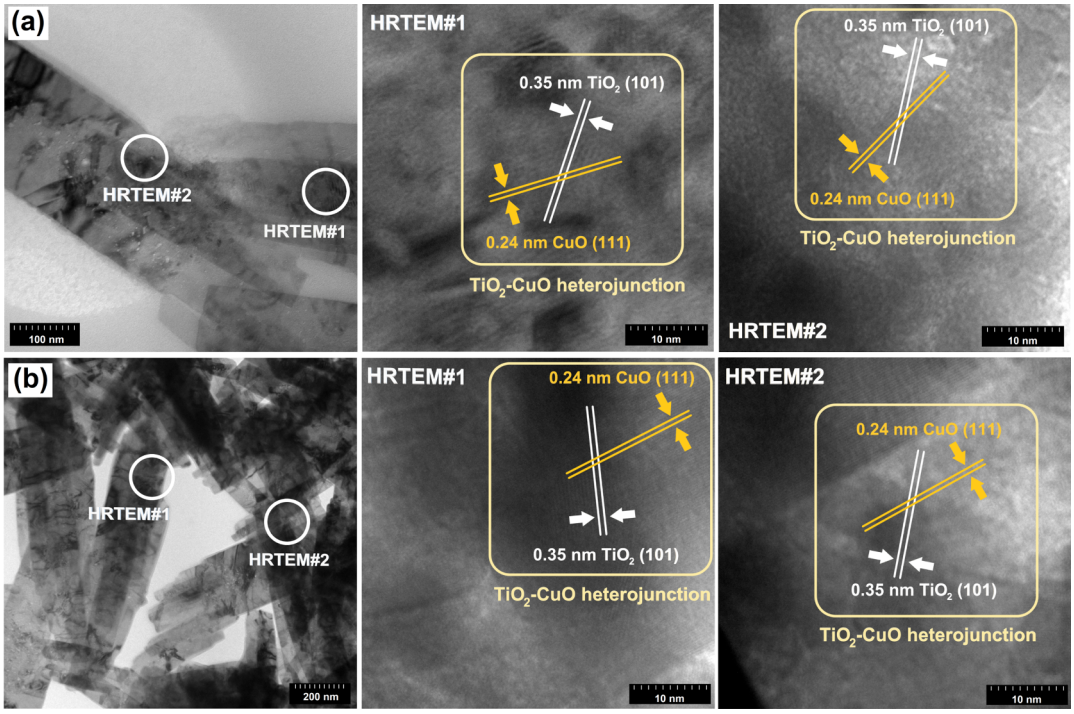

Fig. 3. TEM and HRTEM images for (a) (7)TiO_2-(3)CuO and (b) (3)TiO_2-(7)CuO samples.

Ti 2p, O 1s, and Cu 2p, respectively, are presented in Fig. 6. The Ti 2p region at the TiO_2 material spectrum (see Fig. 6a) shows two characteristic peaks centered at binding energies 458.3 eV and 463.9 eV, which correspond to Ti $2p_{3/2}$ and Ti $2p_{1/2}$ of Ti^{4+} ions in oxide lattice, respectively [55]. No shift of the peaks mentioned above, also no additional peaks may be observed on the spectra of all TiO_2-CuO photocatalysts in the Ti 2p region, which indicates that the addition of CuO is not disturbing the TiO_2 lattice and both oxides exist as separate phases in presented materials [56]. The only observed change in the Ti 2p XPS image is the decrease of intensity of the peaks, which is the natural consequence of the decreasing concentration of the TiO_2 in the materials with the addition of CuO. A similar situation is observed in the Cu 2p region (see Fig. 6b), where typical Cu $2p_{3/2}$ and Cu $2p_{1/2}$ at binding energies of 933.6 eV and 953.5 eV, respectively, may be observed (two additional peaks observed at about 942 eV and 962 eV are satellite peaks typical for Cu^{2+} XPS spectrum [57]). No Cu 2p peaks shifts and no additional peaks are forming when TiO_2 concentration is increasing in the materials presented. The O 1s region (see Fig. 6c) on the spectra of all oxide materials shows a double peak, which after deconvolution may be resolved to two types of oxygen atoms, the lattice oxygen, and adsorbed surface –OH groups. The positions of the O 1s peaks are shifting from 529.4 eV and 531.4 eV to 529.8 eV and 532.1 eV for lattice O and –OH groups, respectively, when the concentration of CuO is increasing in the material, however, no additional peaks may be observed what is supporting our observations described above, that both oxides exist in separated phases.

3.5. Parameters of the porous structure

To determine the parameters of the porous structure, low-

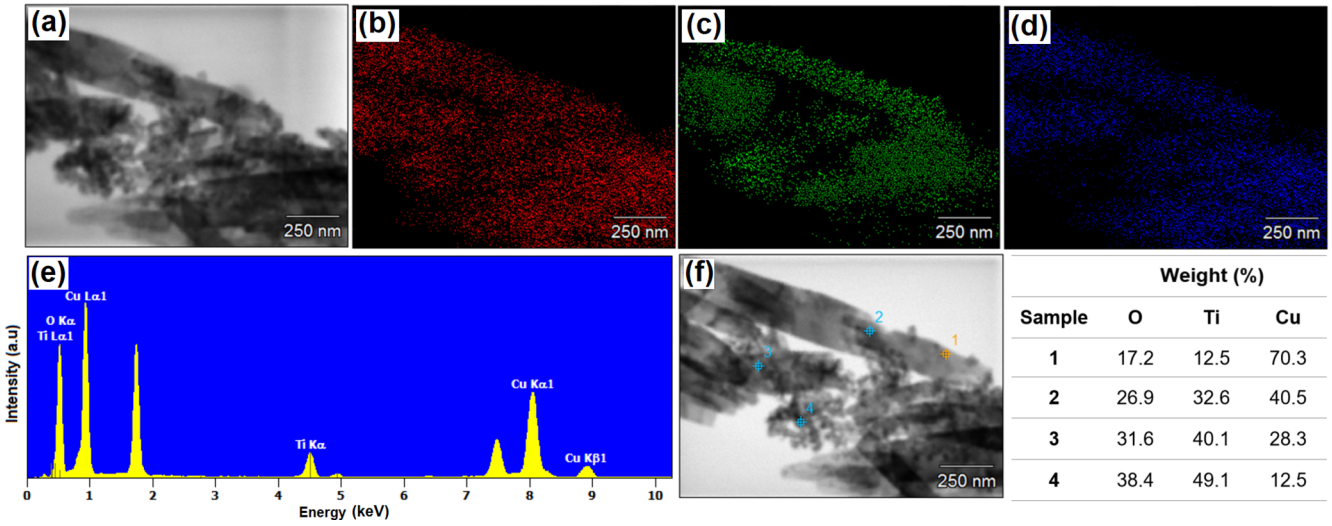

Weight (%)			
Sample	O	Ti	Cu
1	17.2	12.5	70.3
2	26.9	32.6	40.5
3	31.6	40.1	28.3
4	38.4	49.1	12.5

Fig. 4. Microstructure of sample (7)TiO_2-(3)CuO with: (a) STEM image; elemental map of (b) oxygen, (c) titanium, (d) copper; (e) EDS spectrum for mapping and (f) EDS points analysis.

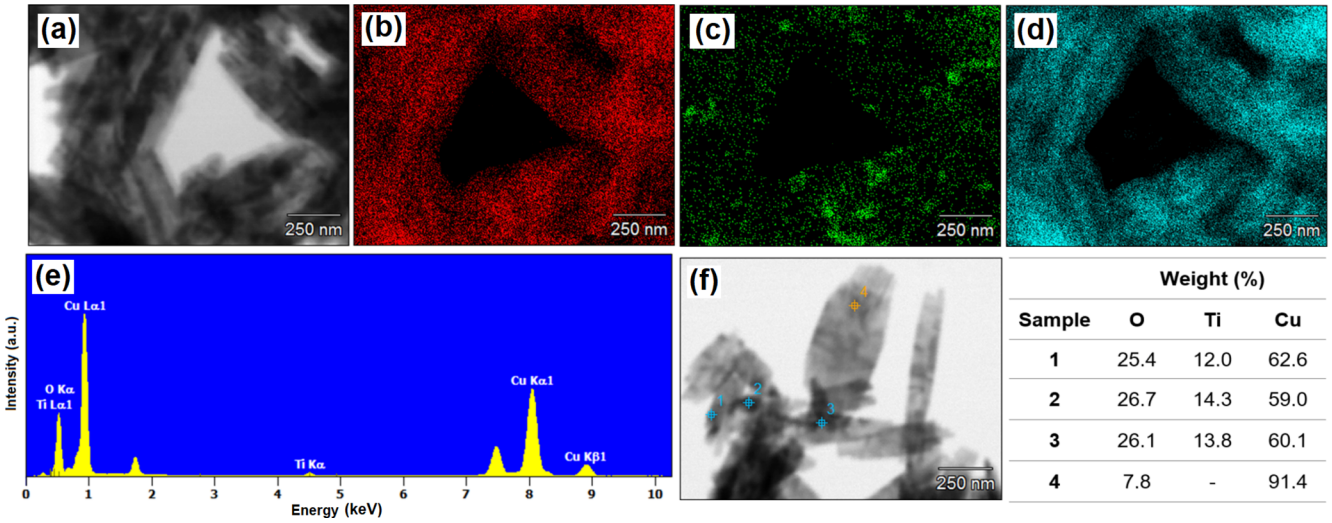

Sample	Weight (%) O	Ti	Cu
1	25.4	12.0	62.6
2	26.7	14.3	59.0
3	26.1	13.8	60.1
4	7.8	-	91.4

Fig. 5. Microstructure of sample (3)TiO_2-(7)CuO with: (a) STEM image; elemental map of (b) oxygen, (c) titanium, (d) copper; (e) EDS spectrum for mapping and (f) EDS points analysis.

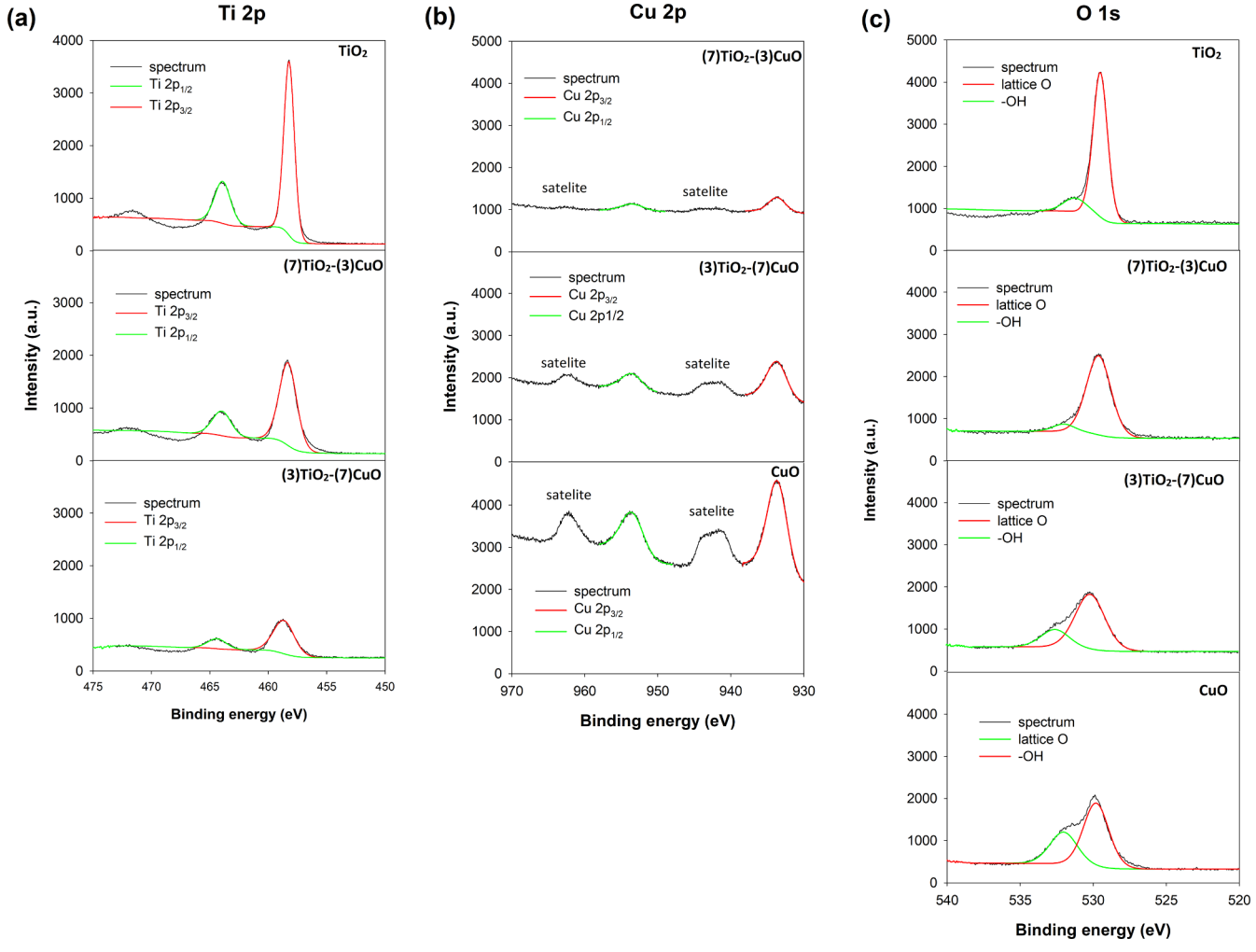

Fig. 6. XPS spectra of specific regions: (a) Ti 2p, (b) Cu 2p and (c) O 1s for reference samples and TiO_2-CuO oxide systems.

temperature nitrogen sorption was used. Fig. 7 shows nitrogen adsorption/desorption isotherms and pore diameter distributions for selected oxide materials.

A type-IV isotherms were observed for both the reference materials and the binary oxide systems. For reference titanium dioxide, an H1 hysteresis loop [58] was observed in a p/p_0 range of 0.65 to 0.98, while for the CuO sample, an H3 hysteresis loop [59] was observed in the range 0.9 to 0.98. Additionally, it should be noted that of all of the analyzed materials, titanium dioxide had the highest surface area (119 m^2/g), and copper(II) oxide the lowest (19 m^2/g). In the

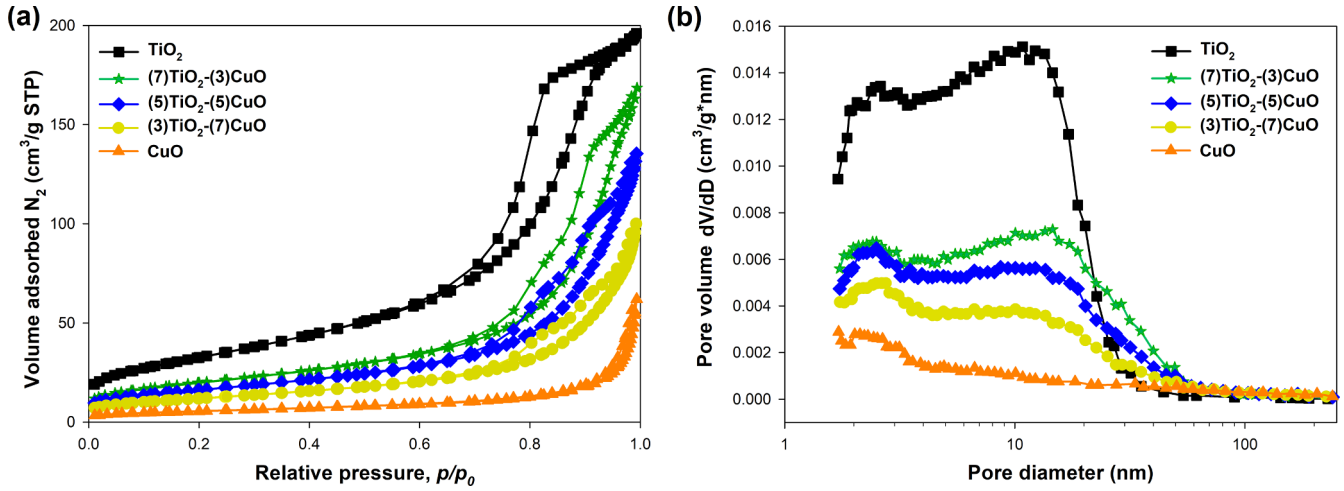

Fig. 7. N_2 adsorption/desorption isotherms (a) and pore diameter distributions (b) of synthesized materials.

adsorption/desorption isotherms for selected oxide systems, H3 hysteresis loops were observed in the ranges 0.65–0.87, 0.68–0.90 and 0.72–0.92 respectively for materials obtained at the molar ratios TiO_2:CuO = 7:3, 5:5 and 3:7. Fig. 7b shows the pore diameter distributions. It was found that only mesopores are present in all of the obtained materials. Moreover, it should be noted that the distribution of pore diameters for the oxide systems is shifted towards higher values compared with the reference titanium dioxide. Additionally, due to the nature of the pore diameter distribution of copper(II) oxide, it should be recognized that the mesopores present in the oxide systems originate mainly from titanium dioxide particles.

Table 2 shows the BET surface area (A_{BET}), pore volume (V_p) and pore diameter (S_p) of the synthesized materials.

It should be noted that the BET results correspond well with the results of the crystalline structure analysis. The decrease in the BET surface area of the oxide system (9)TiO_2-(1)CuO relative to the reference titanium dioxide is caused not only by the addition of copper(II) oxide, but also by an improvement in the crystallinity of the anatase structure, as indicated by the increase in crystallite size, which in turn affects the parameters of the porous structure . Additionally, the low BET surface area obtained for all of the synthesized oxide systems confirms the well-formed crystalline structure of these materials, which is extremely important for future applications. However, it should be noted that for the materials obtained at the molar ratios TiO_2:CuO = 7:3, 5:5 and 3:7, in which highly crystalline anatase and monoclinic CuO structures were observed, the BET surface area is much higher than for the reference CuO. We therefore believe that these materials may be of interest, for example as photocatalytic materials, due to the well-formed crystalline structure and the well-developed porous structure.

In comparing the obtained BET surface area values with those in the existing literature, it should be noted that previously reported materials based on titania and copper(II) oxide were obtained by electrospinning, as described by Lee et al. [31,32] and Zhu et al. [60]. It was observed that binary oxide systems synthesized with molar ratio TiO_2:CuO = 9:3 and 7:3 are characterized with similar textural properties in comparison to materials obtained by electrospinning method by above-mentioned scientists. This fact is due to the presence of highly-crystalline structure of monoclinic copper(II) oxide. In many literature reports in which CuO is synthesized via hydrotehermal or microwave methods the BET surface area is really low. It should be noted, that the copper(II) oxide with flower-like structure fabricated via hydrothermal method by Rezaei et al. [61] and Bhuvaneshwari et al. [62], has surface area about 10 m^2/g.

Table 2
Parameters of porous structure of TiO_2-CuO oxide systems and reference samples.

Sample	A_{BET} (m^2/g)	V_p (cm^3/g)	S_p (nm)
TiO_2	119	0.301	8.6
(9)TiO_2-(1)CuO	75	0.283	10.2
(7)TiO_2-(3)CuO	72	0.251	12.8
(5)TiO_2-(5)CuO	59	0.208	13.1
(3)TiO_2-(7)CuO	43	0.152	13.3
(1)TiO_2-(9)CuO	28	0.113	15.2
CuO	19	0.094	19.7

3.6. Thermal stability

The thermal stability of oxide materials is a very important parameter which may determine their suitability for use in many applications. Results of TGA/DTA analysis are presented in Fig. 8.

For a TiO_2 sample, the total mass loss is about 4% and is associated with the removal of surface-bound water (in the temperature range 50–250 °C). The DTA curve indicates two endothermic peaks associated with the removal of free and surface water. For the reference copper(II) oxide, two mass losses (endothermic peaks) were observed in the temperature ranges 200–250 °C (2%) and 850–900 °C (10%), associated with the removal of surface-bound water and with the CuO to Cu_2O phase transition. The phase transition from copper(II) oxide to copper (I) oxide in an inert gas atmosphere (nitrogen) has been described by other researchers, such as Son et al. [63] and Svintsitskiy et al. [64]. For all analyzed TiO_2-CuO oxide systems, two losses of mass are observed, resulting from the removal of water and the CuO to Cu_2O phase transition. The DTA curves indicate that all mass losses are associated with endothermal transformation. The total mass losses of oxide systems obtained at the molar ratios TiO_2:CuO = 9:1, 7:3. 3:7 and 1:9 were respectively 3.2%, 5.5%, 9.1% and 10.8%. Note should be taken of the influence of the molar ratio on the thermal stability of TiO_2-CuO oxide systems. An increase in the content of copper(II) oxide improves thermal stability in the temperature range 20–800 °C, while in the 800–1000 °C range there is a decrease in thermal stability compared with the TiO_2 reference sample. All of the analyzed materials exhibited good thermal stability up to 1000 °C, which is consistent with the existing literature [65].

3.7. Photocatalytic activity of TiO_2-CuO oxide materials

The study included an evaluation of the photocatalytic activity of the TiO_2-CuO oxide systems in the degradation of tetracycline under UV irradiation. Evaluation of photocatalytic activity was performed for all

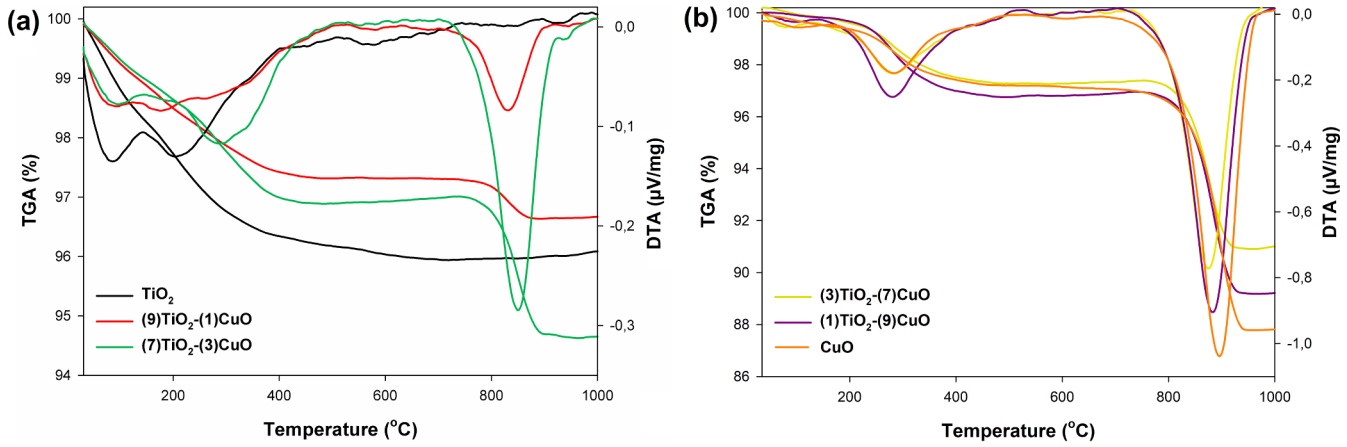

Fig. 8. TGA/DTA curves for materials obtained at TiO_2:CuO molar ratios of (a) 10:0, 9:1, 7:3 and (b) 3:7, 1:9, 0:10.

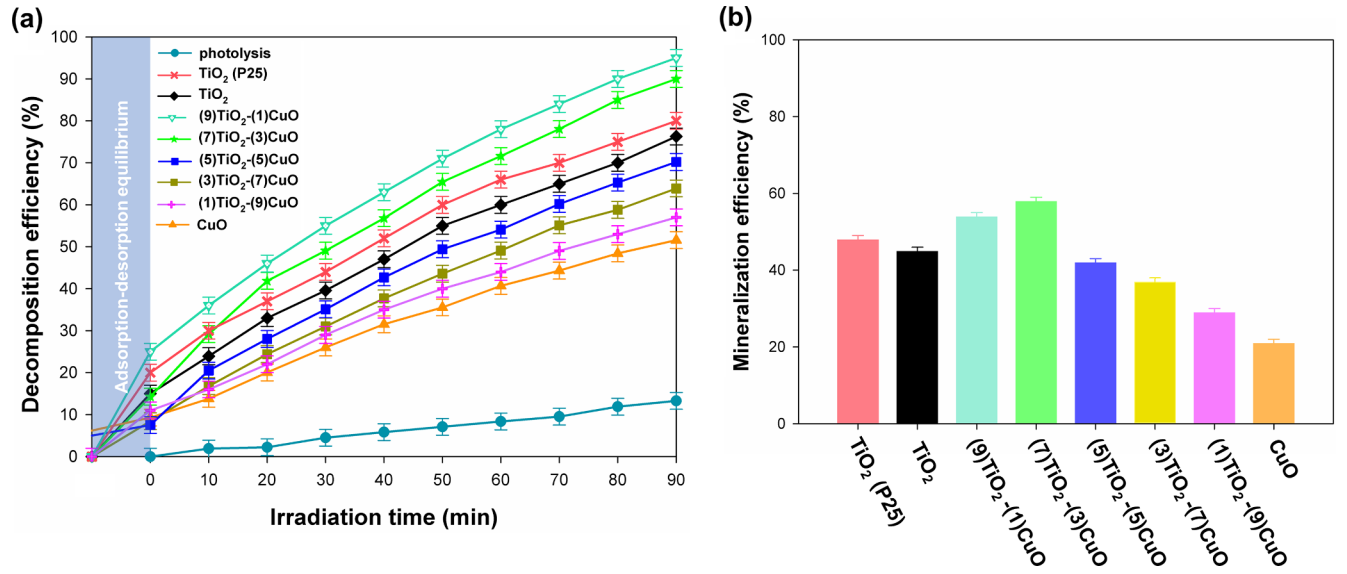

Fig. 9. Efficiency of photocatalytic: (a) decomposition and (b) mineralization of tetracycline in the presence of tested oxide systems.

TiO_2-CuO oxide systems. The results are presented in Fig. 9a.

Initially, it was found that the efficiency of tetracycline decomposition under the action of UV light only is approximately 10% in a time of 90 min. For the reference samples, good photocatalytic activity was demonstrated: the decomposition efficiency was 75% for TiO_2 and 52% for CuO. For TiO_2 the highest adsorption yield of 16% was obtained, which may be due to the well-developed mesoporous structure. For the binary oxide materials obtained at the molar ratios TiO_2:CuO = 1:9, 3:7 and 5:5, the decomposition efficiencies were 57%, 63% and 70% respectively. Highest photocatalytic activity was reported for (9)TiO_2-(1)CuO and (7)TiO_2-(3)CuO samples. In the case of (9)TiO_2-(1)CuO photocatalyst the efficiency of tetracycline decomposition was 94%, but it should be noted that, simultaneously, the highest adsorption yield – 26% was observed for this oxide system. Moreover, for analyzed oxide systems, the monoclinic copper(II) oxide phase had smallest crystallite size (11.4 nm), which may influence the adsorption/desorption equilibrium This observation accurately corresponds with work Wang et al. [66] who indicate the effect of particle size on the adsorption and desorption properties of oxide nanoparticles. However, taking into consideration the (7)TiO_2-(3)CuO sample the decomposition and adsorption efficiency were 91% and 17%, respectively. Additionally, it should be noted that the (9)TiO_2-(1)CuO and (7)TiO_2-(3)CuO oxide systems were characterized by better decomposition efficiency of tetracycline in reference to commercial titanium dioxide (P25). Main reason of enhanced of the photocatalytic activity for (9)TiO_2-(1)CuO and (7)TiO_2-(3)CuO photocatalysts is heterojunction of type Z-scheme. Considering the fact that in this work titanium dioxide is in the anatase crystalline phase, the Z-scheme heterojunction is resulting in the generation of charges with stronger redox potential. The roles of heterostructures in photocatalysts were described by Wang et al. [67] who noted that the heterojunction can overcome the drawbacks of semiconductor photocatalysts such as fast charge recombination and the limited visible-light absorption. Moreover, Jo et al. [68] have demonstrated that the heterojunction between g-C_3N_4 and TiO_2 significantly influences the photocatalytic efficiency of Z-scheme photocatalysts under reaction conditions. Furthermore, the high efficiency of photocatalytic activity can be related to the crystallinity of materials as well as specific morphology. Based on the Scherrer equation calculations it should be noted, that for (9)TiO_2-(1)CuO and (7)TiO_2-(3)CuO materials we can observed the similar crystallite size for both crystalline phase – anatase and monoclinic copper(II) oxide. In the available literature, numerous research groups have indicated that the particle morphology can influence on photocatalytic activity. Shi et al. [49] described the deposition of CuO nanoparticles on anatase nanosheets, what contributes to the inhibition of photoinduced charge carrier recombination effect. Hariganesh et al. [69] have shown that CuO uniformly dispersed in the $CuCr_2O_4$ matrix enables the improvement of photodegradation efficiency against methylene blue and tetracycline. It

has been found that, taking into consideration the obtained morphology of TiO_2-CuO oxide systems, the placement of TiO_2 nanocrystalline particles on CuO sheets can improve the photocatalytic performers. We also observed that photocatalytic decomposition of tetracycline in the presence of commercial titania P25 has a higher efficiency with respect to synthesized TiO_2 (only anatase crystalline structure). The higher degradation yield of tetracycline in presence of commercial titania (P25) in comparison to obtained sample TiO_2 is associated due to the formation of heterojunction between anatase and rutile crystalline structure in the P25, what is described in literature knowledge [19,20]. Moreover, it is worth to add that the decrease of the photocatalytic activity in the case of oxide systems synthesized at molar ratio TiO_2:CuO = 5:5, 3:7 and 1:9 results among others from the increase of charge carriers recombination effect [70] and the shielding effect – the high content of CuO can cause the increase in the opacity and light scattering influencing adversely photon absorption [71]. However, these types of materials can be used e.g., as antibacterial agents [72] or gas sensors [30].

In order to determine the mineralization efficiency the total organic carbon measurement was carried out. Based on the presented results (see Fig. 9b) it was found the similar tendency as compared to above-mentioned decomposition efficiency of tetracycline. The highest mineralization yield of 55% and 60% was reported for (9)TiO_2-(1)CuO and (7)TiO_2-(3)CuO samples, respectively. For others analyzed TiO_2-CuO oxide systems the degree of mineralization were – 42% for (5)TiO_2-(5)CuO, 36% for (3)TiO_2-(7)CuO and 29% for (1)TiO_2-(9)CuO. Moreover, for the reference samples – titanium dioxide and copper(II) oxide – the efficiency of mineralization were 45% and 21%, respectively. It should be mentioned that for commercial P25 titanium dioxide the TOC measurement was 50%. The difference between the decomposition of tetracycline and the degree of mineralization was associated with the formation of photodegradation products.

Furthermore, the TiO_2-CuO photocatalyst with the highest mineralization efficiency ((7)TiO_2-(3)CuO sample) was selected for reusability studies. To evaluate the effectiveness of the photocatalyst after its recovery, five successive cycles were carried out. The data are shown in Fig. 10.

At the end of the first run of photodegradation, (7)TiO_2-(3)CuO oxide systems were separated from the aqueous solution by filtration. The separated photocatalyst was then reused without any treatment. High photocatalytic decomposition of tetracycline was recorded over five consecutive cycles, with an efficiency of 80% in the fifth cycle.

Because tetracycline is a very common pollutant, many groups of researchers are working on its photocatalytic degradation. Table 3 presents the current state of knowledge on the photodegradation of tetracycline using various photocatalysts.

Wang et al. [73] obtained titania-based materials tridoped with C-N-S using the sol-gel method. A high efficiency of photodegradation of tetracycline (98%) after 3 h of visible light irradiation was obtained. Ahmadi et al. [74] showed that MWCNT/TiO_2 nanocomposites can work as effective and convenient photocatalysts for removing tetracycline from wastewater through a degradation process. The use of nano-TiO_2 by Zhu et al. [75] enabled high photoactivity in tetracycline degradation after 40 min. Shi et al. [76] found that a synthesized TiO_2-Cu_2O oxide system exhibited significant photocatalytic activity in the degradation of tetracycline in aqueous solution. Palominos et al. [77] used pure oxides – TiO_2 and ZnO – for the photocatalytic oxidation of tetracycline, determining the effect of the quantity of photocatalyst and the pH on the efficiency of the photodegradation process. Zhang et al. [78] prepared WO_3 and WO_3/Pt materials by a hydrothermal method. They evaluated the photocatalytic activity of the synthesized WO_3/Pt in the photodecomposition of tetracycline under solar light irradiation, and found that it exhibited better photocatalytic activity than bare WO_3 samples. Li et al. [79] obtained a photocatalytically active CdS-TiO_2 heterostructure composite by a hydrothermal method. It achieved a photodegradation efficiency of 87% under visible light irradiation, significantly increased compared with pure TiO_2 and commercial TiO_2 (P25). Chen et al. [80] reported that nanocrystalline AgI/$BiVO_4$ synthesized by an in situ precipitation procedure can be used as a potential photocatalyst in the treatment of tetracycline in wastewater. Wang et al. [81] synthesized PAN/TiO_2/Ag mats using the electrospinning method, and used them in an effective photodegradation process of tetracycline, obtaining a high yield after 240 min.

To describe the mechanism of UV-induced photocatalytic activity of TiO_2-CuO in the oxidative reaction systems, one can distinguish three mechanistic routes: p-n heterojunction of type I or II and Z-scheme

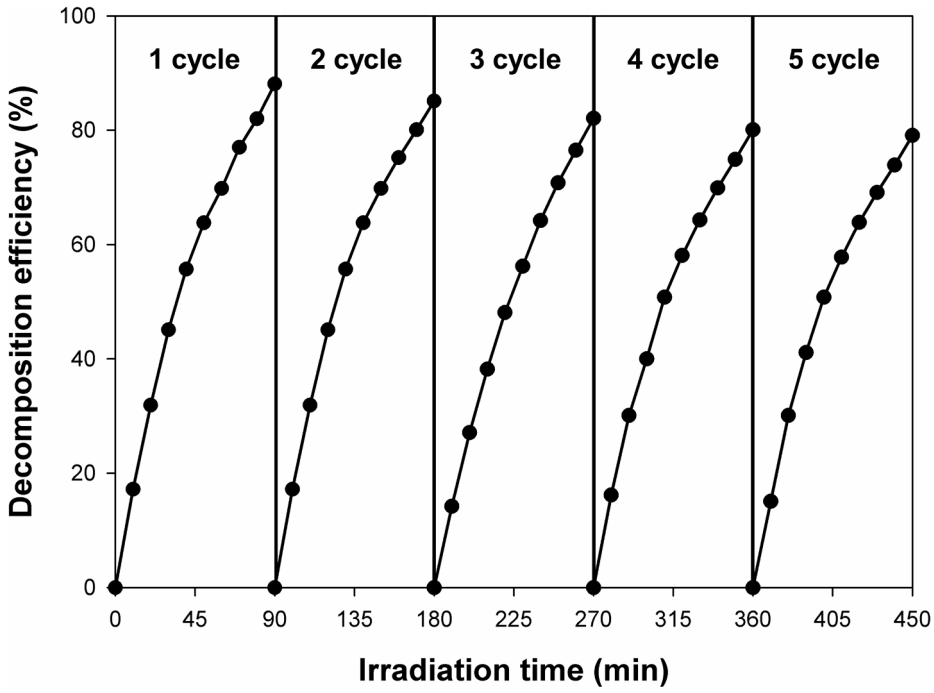

Fig. 10. Efficiency of tetracycline decomposition in the presence of (7)TiO_2-(3)CuO photocatalyst measured over five successive cycles.

Table 3
Efficiency of decomposition of tetracycline using different materials.

Sample	Concentration of pollutant solution (mg/L)	Catalyst amount (mg/100 mL)	Efficiency of decomposition of tetracycline (%)	Time of photodegradation (min)	Ref.
(9)TiO_2-(1)CuO (7)TiO_2-(3)CuO	50	100	95–91	90	This work
TiO_2 doped with C-N-S	5	50	98	180	[73]
MWCNTs/TiO_2	0.5–30	100–400	73–98	20–120	[74]
nano-TiO_2	40	100	95	60	[75]
Cu_2O-TiO_2	30	50	81	120	[76]
ZnO	20	100	95	30	[77]
WO_3	20	100	77	60	[78]
CdS-TiO_2	50	50	87	480	[79]
AgI/$BiVO_4$	20	30	94	60	[80]
PAN/TiO_2/Ag	20	100	95	240	[81]

[19,20]. The mechanism of the photodegradation reaction based on the heterojunction of type I has been described by Moniz et al. [82], who synthesized TiO_2(P25)-CuO photoactive materials, showed that irradiation under UV light caused excitation of titania, and photogenerated electrons were transferred from the valence band (VB) of TiO_2 to the conduction band (CB) of CuO, followed by transfer of photo-excited holes from TiO_2 to the surface for the expected oxidation reactions (p-n heterojunction of type I). The band positions of two semiconductors forming a heterojunction couple influence the type of p-n heterojunction (I or II) [20]. Therefore, according to reported CuO and TiO_2 band positions [20] the heterojunction should be described rather as a type II. Janczarek et al. [19] proposed the mechanism of photodegradation using TiO_2-Cu_2O materials, noting that under UV light irradiation, both Cu_2O and TiO_2 could be excited, or photogenerated electrons in TiO_2 could recombine with photogenerated holes in the VB of Cu_2O. This mechanism is specified for Z-scheme system. That team also found that photocatalytic activity for the oxidation reactions depends directly on the oxidation potential of the holes, as it was also described by Buchalska et al. [83], who demonstrated that anatase was a stronger oxidant than rutile, due to the more positive position of the VB. Therefore, considering the fact that in this work titania is in the anatase form, Z-scheme system is more preferred resulting in the generation of charges with stronger redox potential. The mechanism based on the Z-scheme has also a positive effect on the stability of titania-copper oxide system due to limited photocorrosion of CuO [19]. Moreover, Siah et al. [84] found that CuO clusters can mask the surface of titania, preventing the light source from reaching active sites. Furthermore, CuO clusters in highly CuO-loaded TiO_2 may also act as recombination centers [84]. It has been proven that a determining factor for the photo-oxidation of 2,4-dichlorophenoxyacetic acid is access to the titania surface. On the basis of above-mentioned considerations we propose a possible mechanism for the photodegradation of the model organic pollutant (tetracycline) in the presence of the synthesized TiO_2-CuO materials (Fig. 11).

Under UV irradiation, both CuO and TiO_2 are excited and photogenerated electrons from the CB of TiO_2 recombine with photogenerated holes deriving from the VB of CuO resulting in the formation of more negative electrons and more positive holes and this transfer can occur directly between the semiconductors due to the favorable energetics of the relative positions of CB (TiO_2) and VB (CuO). The oxidation process depends on the holes in the VB of titania reacting with adsorbed water or surface hydroxyl groups to produce hydroxyl radicals. The reduction process occurs at the CB of CuO, where transfer to the dissolved oxygen takes place, producing superoxide anion radicals which may be transformed into active oxygen species.

Based on the previous scientific reports in particular Ohtani [85] and Amano et al. [86] works, the type of single-crystalline structure of titania (particle morphology) has been recognized as an important physicochemical property influencing photocatalytic activity. Additionally, it should be noted, that crystallinity determines the photocatalytic efficiency, however various materials with different particle shape can be characterized by the similar crystalline properties. Verrbrunggen [87] and Wang et al. [88] described that design of particle morphology is one of the most important steps for plasmonic enhancement of titanium dioxide photocatalysts. Ola et al. [89] indicated that the different morphological and textural properties lead to improve or deterioration of photocatalytic activity. However, the authors paid attention that titania modification and the type of synthesis method play a key role in the design of photocatalytic properties of final materials.

Many researchers have been focused on the modification of titanium dioxide with synthesized oxide systems – particularly TiO_2-CuO oxide systems. Rokhmat et al. [90] prepared TiO_2-CuO materials via spraying process of TiO_2-CuO suspension to the Fluorin doped Tin Oxide (FTO). The authors used obtained materials in dye sensitized solar cells (DSSC). It was found that the optimal content of copper(II) oxide was 7.93%. Luna et al. [91] used the impregnation method for synthesis TiO_2-CuO photocatalysts. Furthermore, it was found that the prepared materials were characterized by three crystalline phases: anatase, CuO and Cu_2O. Additionally, the high photodegradation efficiency of gallic acid for analyzed materials was observed. Moreover, the incorporation of copper oxide to TiO_2 significantly decreases the band gap energy (E_g = 2.06 for 70% CuO). Moniz et al. [82] used the solvothermal microwave method for synthesis titania(P25)-copper(II) oxide materials. The Authors show that the largest increase of mineralization of 2,4-dichlorophenoxyacetic acid was exhibited by the 5% and 10% CuO-P25 sample. Chu et al. [92] prepared Cu_2O@TiO_2 core–shell heterojunction photocatalyst by an in situ hydrolysis and crystallization method. They found that core-shell structure plays a crucial role in the improvement of photocatalytic properties in 4-nitrophenol degradation.

According with above-mentioned literature it should be noted that the following parameters such as: content of CuO, crystallinity, morphology and band gap energy influence the photocatalytic activity of TiO_2-CuO materials. Similar thesis was presented in review articles by Janczarek et al. [20] and Wei et al. [88].

Comparing the results obtained in this work with the available scientific knowledge, it should pay attention that the photocatalytic properties of obtained oxide systems were correlated with the same parameters that were described in the literature. However, our results of tetracycline degradation showed better photocatalytic performance than described in the literature, due to the application of microwave-assisted synthesis. The microwave irradiation enables obtaining small particles [40], designing morphology [44] and forming well-formed crystalline structure without calcination [39]. Additionally, the Researchers [93,94] found that the microwave-assisted synthesis allows to obtain heterojunction in the materials based on oxides, what influence on the improve the photocatalytic performances. Moreover, the microwave-assisted synthesis more shortens the process time what's important with practical aspects. Oghbaei et al. [95] described that the microwave-assisted synthesis, also consumes much lower energy than

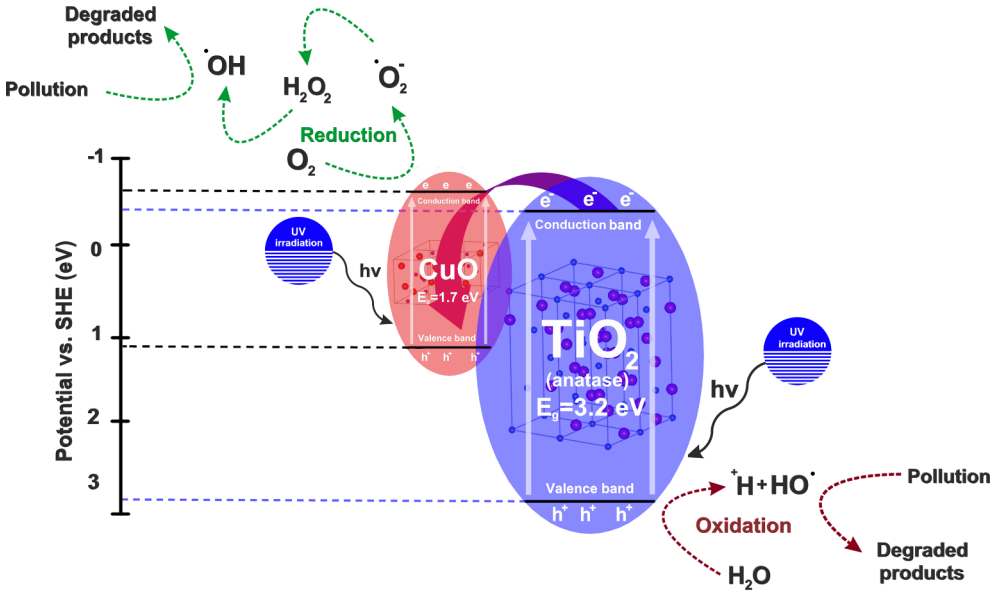

Fig. 11. The proposed mechanism of photocatalytic degradation of organic impurity in the presence of oxide materials.

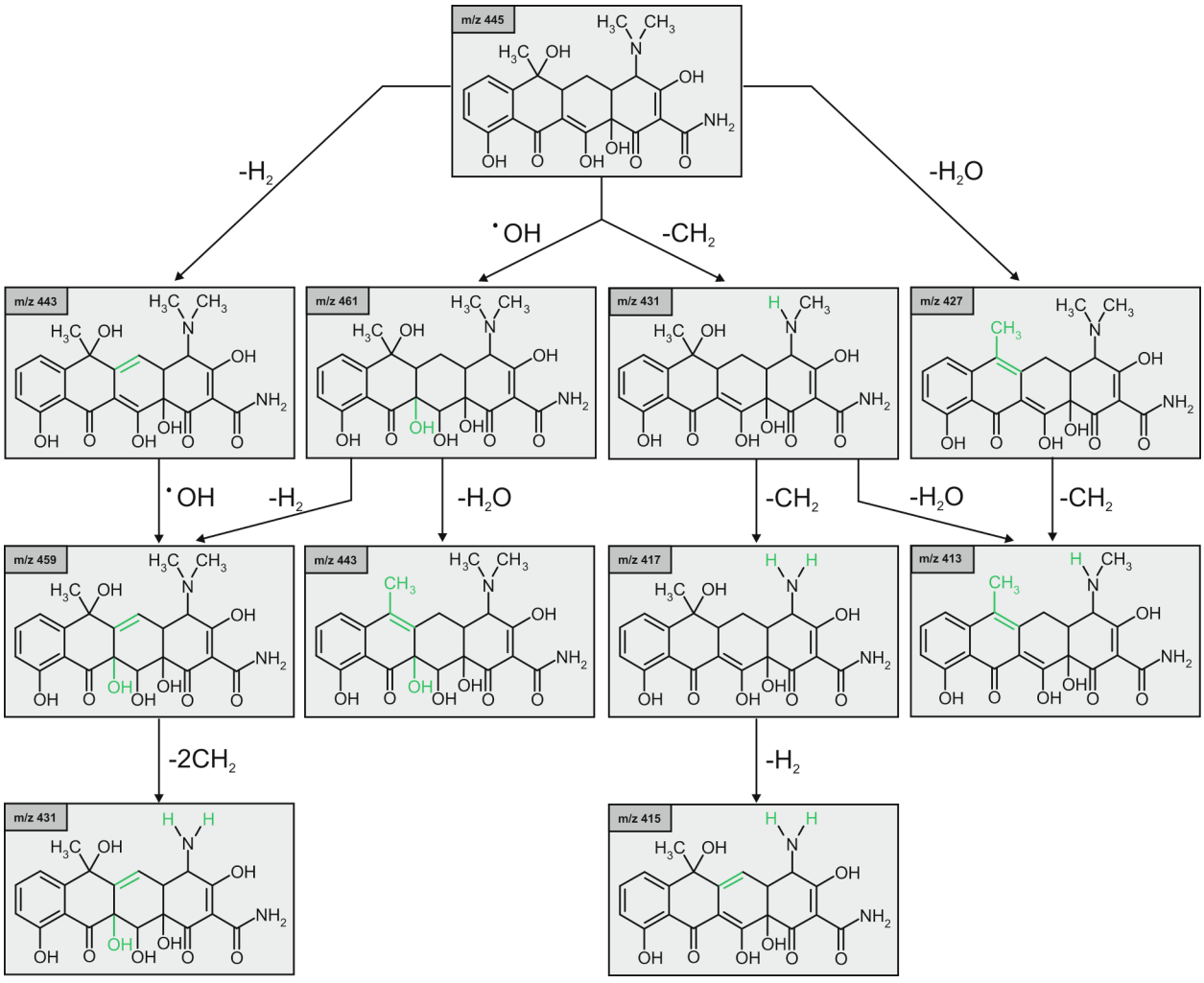

Fig. 12. Degradation scheme of tetracycline, with *m/z* values of protonated molecules given by the structures of compounds.

conventional methods as well as diffusion processes intensifies by using microwave irradiation. Furthermore, the Roberts and Strauss [96] indicate that the microwave synthesis can be elements of a broad strategy toward environmentally.

3.8. Identification of degradation products

A key element of the present work was the determination of tetracycline photodegradation products using the HPLC/MS technique (Fig. 12). During the photocatalytic degradation of tetracycline, four processes were observed: oxidation, dehydration, dehydrogenation and demethylation. Different degradation pathways can be found depending on the sequence of degradation processes. A number of products were found during the study (Fig. 12) irrespective of the ratio of TiO_2 to CuO in the catalyst. The degradation follows previously described general schemes found in similar processes, with slight differences. Li et al. [97] found only a few degradation products, which indicates that the process used in their laboratory was milder. On the other hand, Deng et al. [98] presented a more advanced photodegradation with numerous oxidation steps. Nevertheless, the catalytic system proposed by Deng et al. [98] involved a complicated and energy-consuming synthesis processes, carried out for many hours at 500–550 °C, which would be difficult to commercialize. Due to the complexity of the products obtained following photodegradation, further investigation is still in progress.

4. Conclusions

The main objective of this work was the synthesis of a TiO_2-CuO oxide system using a microwave method. The use of a synthesis method not previously reported for this material led to oxide systems with well-formed crystalline structures of both anatase and monoclinic CuO. Furthermore, rod-shaped particles of TiO_2 and sheet particles of CuO were observed. In the resulting TiO_2-CuO oxide systems, it was determined that TiO_2 nanoparticles were present on CuO sheets, which resulted in a surface junction. It was found that physicochemical properties such as crystalline structure, parameters of the porous structure, surface composition and thermal stability of the binary oxide systems are strongly dependent on the molar ratio of the reagents used in their preparation.

A key element of the research was the evaluation of the efficiency of photodegradation of the organic pollutant – tetracycline – in the presence of the synthesized binary oxide materials. It was proved that the TiO_2-CuO oxide materials (especially samples (9)TiO_2-(1)CuO (7)TiO_2-(3)CuO) exhibit high photocatalytic activity in the decomposition of tetracycline. The Z-scheme is indicated as the basis of the proposed photocatalytic reaction mechanism. Furthermore, during the photocatalytic degradation of tetracycline, four processes were observed: oxidation, dehydration, dehydrogenation and demethylation. The results show that the synthesized TiO_2-CuO oxide systems are promising materials for photocatalytic applications.

CRediT authorship contribution statement

Adam Kubiak: Conceptualization, Methodology, Investigation, Data curation, Writing - original draft. **Zuzanna Bielan:** Formal analysis, Data curation. **Marta Kubacka:** Validation, Data curation. **Elżbieta Gabała:** Formal analysis, Investigation. **Agnieszka Zgoła-Grześkowiak:** Formal analysis, Investigation. **Marcin Janczarek:** Data curation, Investigation. **Maciej Zalas:** Investigation, Visualization. **Anna Zielińska-Jurek:** Writing - review & editing. **Katarzyna Siwińska-Ciesielczyk:** Writing - review & editing. **Teofil Jesionowski:** Supervision, Project administration, Funding acquisition, Writing - review & editing.

Declaration of Competing Interest

The authors declare that they have no known competing financial interests or personal relationships that could have appeared to influence the work reported in this paper.

Acknowledgements

This research was funded by Polish Ministry of Science and Higher Education research grant no. 0912/SBAD/2006.

References

[1] M. Lilenberg, S. Yurchenko, K. Kipper, K. Herodes, V. Pihl, K. Sepp, R. Lohmus, L. Nei, Simultaneous determination of fluoroquinolones, sulfonamides and tetracyclines in sewage sludge by pressurized liquid extraction and liquid chromatography electrospray ionization-mass spectrometry, J. Chromatogr. A. 1216 (2009) 5949–5954, https://doi.org/10.1016/j.chroma.2009.06.029.
[2] S. Fekadu, E. Alemayehu, R. Dewil, B. Van der Bruggen, Pharmaceuticals in freshwater aquatic environments: A comparison of the African and European challenge, Sci. Total Environ. 654 (2019) 324–337, https://doi.org/10.1016/j.scitotenv.2018.11.072.
[3] J. Lyu, Z. Hu, Z. Li, M. Ge, Removal of tetracycline by BiOBr microspheres with oxygen vacancies: Combination of adsorption and photocatalysis, J. Phys. Chem. Solids. 129 (2019) 61–70, https://doi.org/10.1016/j.jpcs.2018.12.041.
[4] J. Martín, M.D. Camacho-Muñoz, J.L. Santos, I. Aparicio, E. Alonso, Distribution and temporal evolution of pharmaceutically active compounds alongside sewage sludge treatment. Risk assessment of sludge application onto soils, J. Environ. Manage. 102 (2012) 18–25, https://doi.org/10.1016/j.jenvman.2012.02.020.
[5] L. Pasquini, J.F. Munoz, M.N. Pons, J. Yvon, X. Dauchy, X. France, N.D. Le, C. France-Lanord, T. Görner, Occurrence of eight household micropollutants in urban wastewater and their fate in a wastewater treatment plant, Statistical Evaluation, Sci. Total Environ. 481 (2014) 459–468, https://doi.org/10.1016/j.scitotenv.2014.02.075.
[6] T. Deblonde, C. Cossu-Leguille, P. Hartemann, Emerging pollutants in wastewater: A review of the literature, Int. J. Hyg. Environ. Health. 214 (2011) 442–448, https://doi.org/10.1016/j.ijheh.2011.08.002.
[7] H.B. Quesada, A.T.A. Baptista, L.F. Cusioli, D. Seibert, C. de Oliveira Bezerra, R. Bergamasco, Surface water pollution by pharmaceuticals and an alternative of removal by low-cost adsorbents: A review, Chemosphere 222 (2019) 766–780, https://doi.org/10.1016/j.chemosphere.2019.02.009.
[8] W. Peysson, E. Vulliet, Determination of 136 pharmaceuticals and hormones in sewage sludge using quick, easy, cheap, effective, rugged and safe extraction followed by analysis with liquid chromatography-time-of-flight-mass spectrometry, J. Chromatogr. A. 1290 (2013) 46–61, https://doi.org/10.1016/j.chroma.2013.03.057.
[9] J.L. Liu, M.H. Wong, Pharmaceuticals and personal care products (PPCPs): A review on environmental contamination in China, Environ. Int. 59 (2013) 208–224, https://doi.org/10.1016/j.envint.2013.06.012.
[10] M. Topal, E.I. Arslan Topal, Investigation of tetracycline and degradation products in Euphrates river receiving outflows of trout farms, Aquac. Res. 47 (2016) 3837–3844, https://doi.org/10.1111/are.12834.
[11] Y. Zhang, S. Zuo, M. Zhou, L. Liang, G. Ren, Removal of tetracycline by coupling of flow-through electro-Fenton and in-situ regenerative active carbon felt adsorption, Chem. Eng. J. 335 (2018) 685–692, https://doi.org/10.1016/j.cej.2017.11.012.
[12] J. Yu, J. Kiwi, I. Zivkovic, H.M. Rønnow, T. Wang, S. Rtimi, Quantification of the local magnetized nanotube domains accelerating the photocatalytic removal of the emerging pollutant tetracycline, Appl. Catal. B Environ. 248 (2019) 450–458, https://doi.org/10.1016/j.apcatb.2019.02.046.
[13] G.M. Islam, K.A. Gilbride, The effect of tetracycline on the structure of the bacterial community in a wastewater treatment system and its effects on nitrogen removal, J. Hazard. Mater. 371 (2019) 130–137, https://doi.org/10.1016/j.jhazmat.2019.02.032.
[14] J.D. Toth, Y. Feng, Z. Dou, Veterinary antibiotics at environmentally relevant concentrations inhibit soil iron reduction and nitrification, Soil Biol. Biochem. 43 (2011) 2470–2472, https://doi.org/10.1016/j.soilbio.2011.09.004.
[15] H. Zhang, P. Liu, Y. Feng, F. Yang, Fate of antibiotics during wastewater treatment and antibiotic distribution in the effluent-receiving waters of the Yellow Sea, northern China, Mar. Pollut. Bull. 73 (2013) 282–290, https://doi.org/10.1016/j.marpolbul.2013.05.007.
[16] P. Guerra, M. Kim, A. Shah, M. Alaee, S.A. Smyth, Occurrence and fate of antibiotic, analgesic/anti-inflammatory, and antifungal compounds in five wastewater treatment processes, Sci. Total Environ. 473–474 (2014) 235–243, https://doi.org/10.1016/j.scitotenv.2013.12.008.
[17] K.G. Karthikeyan, M.T. Meyer, Occurrence of antibiotics in wastewater treatment facilities in Wisconsin, USA, Sci. Total Environ. 361 (2006) 196–207, https://doi.org/10.1016/j.scitotenv.2005.06.030.
[18] J. Cao, Z. Xiong, B. Lai, Effect of initial pH on the tetracycline (TC) removal by zero-valent iron: Adsorption, oxidation and reduction, Chem. Eng. J. 343 (2018) 492–499, https://doi.org/10.1016/j.cej.2018.03.036.
[19] M. Janczarek, M. Endo, D. Zhang, K. Wang, E. Kowalska, Enhanced photocatalytic

and antimicrobial performance of cuprous oxide/titania: the effect of titania matrix, Materials 11 (2018) 2069, https://doi.org/10.3390/ma11112069.
[20] M. Janczarek, E. Kowalska, On the origin of enhanced photocatalytic activity of copper-modified titania in the oxidative reaction systems, Catalysts 7 (2017) 317, https://doi.org/10.3390/catal7110317.
[21] C. McCullagh, J.M.C. Robertson, D.W. Bahnemann, P.K.J. Robertson, The application of TiO_2 photocatalysis for disinfection of water contaminated with pathogenic micro-organisms: A review, Res. Chem. Intermed. 33 (2007) 359–375, https://doi.org/10.1163/156856707779238775.
[22] B. Roose, S. Pathak, U. Steiner, Doping of TiO_2 for sensitized solar cells, Chem. Soc. Rev. 44 (2015) 8326–8349, https://doi.org/10.1039/c5cs00352k.
[23] I.P. Parkin, R.G. Palgrave, Self-cleaning coatings, J. Mater. Chem. 15 (2005) 1689–1695, https://doi.org/10.1039/b412803f.
[24] H. Wu, Y. Yang, H. Suo, M. Qing, L. Yan, B. Wu, J. Xu, H. Xiang, Y. Li, Effects of ZrO_2 promoter on physic-chemical properties and activity of Co/TiO_2–SiO_2 Fischer-Tropsch catalysts, J. Mol. Catal. A Chem. 396 (2014) 108–119, https://doi.org/10.1016/j.molcata.2014.09.024.
[25] B. Ohtani, Titania photocatalysis beyond recombination: A critical review, Catalysts 3 (2013) 942–953, https://doi.org/10.3390/catal3040942.
[26] M. Fujishima, H. Takatori, H. Tada, Interfacial chemical bonding effect on the photocatalytic activity of TiO_2-SiO_2 nanocoupling systems, J. Colloid Interface Sci. 361 (2011) 628–631, https://doi.org/10.1016/j.jcis.2011.06.024.
[27] R. Asahi, T. Morikawa, T. Ohwaki, K. Aoki, Y. Taga, Visible-light photocatalysis in nitrogen-doped titanium oxides, Science 293 (2001) 269–271, https://doi.org/10.1126/science.1061051.
[28] M. Pelaez, N.T. Nolan, S.C. Pillai, M.K. Seery, P. Falaras, A.G. Kontos, P.S.M. Dunlop, J.W.J. Hamilton, J.A. Byrne, K. O'Shea, M.H. Entezari, D.D. Dionysiou, A review on the visible light active titanium dioxide photocatalysts for environmental applications, Appl. Catal. B 125 (2012) 331–349, https://doi.org/10.1016/j.apcatb.2012.05.036.
[29] F. Yang, X. Zhang, Y. Yang, S. Hao, L. Cui, Characteristics and supercapacitive performance of nanoporous bamboo leaf-like CuO, Chem. Phys. Lett. 691 (2018) 366–372, https://doi.org/10.1016/j.cplett.2017.11.047.
[30] K. Zhang, Q. Zhang, D. Xu, G. Yang, H. Huang, F. Nie, C. Liu, S. Yang, CuO nanostructures: Synthesis, characterization, growth mechanisms, fundamental properties, and applications, Prog. Mater. Sci. 60 (2014) 208–237, https://doi.org/10.1016/j.pmatsci.2013.09.003.
[31] S.S. Lee, H. Bai, Z. Liu, D.D. Sun, Novel-structured electrospun TiO_2/CuO composite nanofibers for high efficient photocatalytic cogeneration of clean water and energy from dye wastewater, Water Res. 47 (2013) 4059–4073, https://doi.org/10.1016/j.watres.2012.12.044.
[32] S.S. Lee, H. Bai, Z. Liu, D.D. Sun, Optimization and an insightful properties-activity study of electrospun TiO_2/CuO composite nanofibers for efficient photocatalytic $_H2$ generation, Appl. Catal. B Environ. 140–141 (2013) 68–81, https://doi.org/10.1016/j.apcatb.2013.03.033.
[33] P. Wang, X. Wen, R. Amal, Y.H. Ng, Introducing a protective interlayer of TiO_2 in Cu_2O-CuO heterojunction thin film as a highly stable visible light photocathode, RSC Adv. 5 (2015) 5231–5236, https://doi.org/10.1039/c4ra13464h.
[34] J. Bandara, C.P.K. Udawatta, C.S.K. Rajapakse, Highly stable CuO incorporated TiO_2 catalyst for photocatalytic hydrogen production from H_2O, Photochem. Photobiol. Sci. 4 (2005) 857–861, https://doi.org/10.1039/b507816d.
[35] S. Qin, F. Xin, Y. Liu, X. Yin, W. Ma, Photocatalytic reduction of CO_2 in methanol to methyl formate over CuO-TiO_2 composite catalysts, J. Colloid Interface Sci. 356 (2011) 257–261, https://doi.org/10.1016/j.jcis.2010.12.034.
[36] J.F. de Brito, M.V.B. Zanoni, On the application of Ti/TiO_2/CuO n-p junction semiconductor: A case study of electrolyte, temperature and potential influence on CO_2 reduction, Chem. Eng. J. 318 (2017) 264–271, https://doi.org/10.1016/j.cej.2016.08.033.
[37] A. Monshi, M.R. Foroughi, M.R. Monshi, Modified Scherrer equation to estimate more accurately nano-crystallite size using XRD, World J. Nano Sci. Eng. 02 (2012) 154–160, https://doi.org/10.4236/wjnse.2012.23020.
[38] A. Khorsand Zak, W.H. Abd Majid, M.E. Abrishami, R. Yousefi, X-ray analysis of ZnO nanoparticles by Williamson-Hall and size-strain plot methods, Solid State Sci. 13 (2011) 251–256, https://doi.org/10.1016/j.solidstatesciences.2010.11.024.
[39] M.I. Dar, A.K. Chandiran, M. Grätzel, M.K. Nazeeruddin, S.A. Shivashankar, Controlled synthesis of TiO_2 nanoparticles and nanospheres using a microwave assisted approach for their application in dye-sensitized solar cells, J. Mater. Chem. A. 2 (2014) 1662–1667, https://doi.org/10.1039/c3ta14130f.
[40] A.B. Corradi, F. Bondioli, B. Focher, A.M. Ferrari, C. Grippo, E. Mariani, C. Villa, Conventional and microwave-hydrothermal synthesis of TiO_2 nanopowders, J. Am. Ceram. Soc. 88 (2005) 2639–2641, https://doi.org/10.1111/j.1551-2916.2005.00474.x.
[41] G.S. Falk, M. Borlaf, M.J. López-Muñoz, J.C. Fariñas, J.B. Rodrigues Neto, R. Moreno, Microwave-assisted synthesis of TiO_2 nanoparticles: photocatalytic activity of powders and thin films, J. Nanoparticle Res. 20 (2018) 23, https://doi.org/10.1007/s11051-018-4140-7.
[42] X. Wang, J. Tian, C. Fei, L. Lv, Y. Wang, G. Cao, Rapid construction of TiO_2 aggregates using microwave assisted synthesis and its application for dye-sensitized solar cells, RSC Adv. 5 (2014) 8622–8629, https://doi.org/10.1039/c4ra11266k.
[43] D.P. Volanti, D. Keyson, L.S. Cavalcante, A.Z. Simões, M.R. Joya, E. Longo, J.A. Varela, P.S. Pizani, A.G. Souza, Synthesis and characterization of CuO flower-nanostructure processing by a domestic hydrothermal microwave, J. Alloys Compd. 459 (2008) 537–542, https://doi.org/10.1016/j.jallcom.2007.05.023.
[44] C. Yang, F. Xiao, J. Wang, X. Su, 3D flower- and 2D sheet-like CuO nanostructures: Microwave-assisted synthesis and application in gas sensors, Sens Actuators, B Chem. 207 (2015) 177–185, https://doi.org/10.1016/j.snb.2014.10.063.
[45] G. Qiu, S. Dharmarathna, Y. Zhang, N. Opembe, H. Huang, S.L. Suib, Facile microwave-assisted hydrothermal synthesis of CuO nanomaterials and their catalytic and electrochemical properties, J. Phys. Chem. C. 116 (2012) 468–477, https://doi.org/10.1021/jp209911k.
[46] M.C. Mathpal, A.K. Tripathi, M.K. Singh, S.P. Gairola, S.N. Pandey, A. Agarwal, Effect of annealing temperature on Raman spectra of TiO_2 nanoparticles, Chem. Phys. Lett. 555 (2012) 182–186, https://doi.org/10.1016/j.cplett.2012.10.082.
[47] K. Phiwdang, S. Suphankij, W. Mekprasart, W. Pecharapa, Synthesis of CuO nanoparticles by precipitation method using different precursors, Energy Proc. 34 (2013) 740–745, https://doi.org/10.1016/j.egypro.2013.06.808.
[48] L. Zhu, M. Hong, G. Wei, Fabrication of wheat grain textured TiO_2/CuO composite nano fibers for enhanced solar H_2 generation and degradation performance, Nano Energy 11 (2015) 28–37, https://doi.org/10.1016/j.nanoen.2014.09.032.
[49] Q. Shi, G. Ping, X. Wang, H. Xu, J. Li, J. Cui, H. Abroshan, H. Ding, G. Li, CuO/TiO_2 heterojunction composites: An efficient photocatalyst for selective oxidation of methanol to methyl formate, J. Mater. Chem. A. 7 (2019) 2253–2260, https://doi.org/10.1039/c8ta09439j.
[50] G. Nagaraju, T. Ramakrishnappa, J.D. Scholten, K. Manjunath, J. Dupont, V.S. Souza, Heterojunction CuO-TiO_2 nanocomposite synthesis for significant photocatalytic hydrogen production, Mater. Res. Express. 3 (2016) 115904, , https://doi.org/10.1088/2053-1591/3/11/115904.
[51] E.P. Etape, L.J. Ngolui, J. Fobatendo, D.M. Yufanyi, B.V. Namondo, Synthesis and characterization of CuO, TiO_2, and CuO-TiO_2 mixed oxide by a modified oxalate route, J. Appl. Chem. 2017 (2017) 4518654, https://doi.org/10.1155/2017/4518654.
[52] A.M. Cahino, R.G. Loureiro, J. Dantas, V.S. Madeira, P.C. Ribeiro Fernandes, Characterization and evaluation of ZnO/CuO catalyst in the degradation of methylene blue using solar radiation, Ceram. Inter. 45 (2019) 13628–13636, https://doi.org/10.1063/1.4945505.
[53] J. Yu, X. Zhao, Q. Zhao, G. Wang, Preparation and characterization of super-hydrophilic porous TiO_2 coating films, Mater. Chem. Phys. 68 (2001) 253–259, https://doi.org/10.1016/S0254-0584(00)00364-3.
[54] S. Rahim, M.S. Ghamsari, S. Radiman, Surface modification of titanium oxide nanocrystals with PEG, Sci. Iran. 19 (2012) 948–953, https://doi.org/10.1016/j.scient.2012.03.009.
[55] M.S. Kim, S.H. Chung, C.J. Yoo, M.S. Lee, I.H. Cho, D.W. Lee, K.Y. Lee, Catalytic reduction of nitrate in water over Pd-Cu/TiO_2 catalyst: Effect of the strong metal-support interaction (SMSI) on the catalytic activity, Appl. Catal. B Environ. 142–143 (2013) 354–361, https://doi.org/10.1016/j.apcatb.2013.05.033.
[56] J.O. Olowoyo, M. Kumar, T. Dash, S. Saran, S. Bhandari, U. Kumar, Self-organized copper impregnation and doping in TiO2 with enhanced photocatalytic conversion of H_2O and CO_2 to fuel, Int. J. Hydrogen Energy. 43 (2018) 19468–19480, https://doi.org/10.1016/j.ijhydene.2018.08.209.
[57] A.A. Dubale, C.J. Pan, A.G. Tamirat, H.M. Chen, W.N. Su, C.H. Chen, J. Rick, D.W. Ayele, B.A. Aragaw, J.F. Lee, Y.W. Yang, B.J. Hwang, Heterostructured Cu_2O/CuO decorated with nickel as a highly efficient photocathode for photoelectrochemical water reduction, J. Mater. Chem. A. 3 (2015) 12482–12499, https://doi.org/10.1039/c5ta01961c.
[58] R. Van Grieken, J. Aguado, M.J. López-Muoz, J. Marugán, Synthesis of size-controlled silica-supported TiO_2 photocatalysts, J. Photochem. Photobiol. A Chem. 148 (2002) 315–322, https://doi.org/10.1016/S1010-6030(02)00058-8.
[59] K. Zhou, R. Wang, B. Xu, Y. Li, Synthesis, characterization and catalytic properties of CuO nanocrystals with various shapes, Nanotechnology. 17 (2006) 3939–3943, https://doi.org/10.1088/0957-4484/17/15/055.
[60] L. Zhu, M. Hong, G.W. Ho, Fabrication of wheat grain textured TiO_2/CuO composite nanofibers for enhanced solar H_2 generation and degradation performance, Nano Energy 11 (2015) 28–37, https://doi.org/10.1016/j.nanoen.2014.09.032.
[61] P. Rezaei, M. Rezaei, F. Meshkani, Ultrasound-assisted hydrothermal method for the preparation of the M-Fe_2O_3-CuO (M: Mn, Ag, Co) mixed oxides nanocatalysts for low-temperature CO oxidation, Ultrason.-Sonochem. 57 (2019) 212–222, https://doi.org/10.1016/j.ultsonch.2019.04.042.
[62] S. Bhuvaneshwari, N. Gopalakrishnan, Hydrothermally synthesized copper oxide (CuO) superstructures for ammonia sensing, J. Colloid Interface Sci. 480 (2016) 76–84, https://doi.org/10.1016/j.jcis.2016.07.004.
[63] S.R. Son, K.S. Go, S.D. Kim, Thermogravimetric analysis of copper oxide for chemical-looping hydrogen generation, Ind. Eng. Chem. Res. 48 (2009) 380–387, https://doi.org/10.1021/ie800174c.
[64] D.A. Svintsitskiy, A.P. Chupakhin, E.M. Slavinskaya, O.A. Stonkus, A.I. Stadnichenko, S.V. Koscheev, A.I. Boronin, Study of cupric oxide nanopowders as efficient catalysts for low-temperature CO oxidation, J. Mol. Catal. A Chem. 368–369 (2013) 95–106, https://doi.org/10.1016/j.molcata.2012.11.015.
[65] N. Tamaekong, C. Liewhiran, S. Phanichphant, Synthesis of thermally spherical CuO nanoparticles, J. Nanomater. 2014 (2014) 1–5, https://doi.org/10.1155/2014/507978.
[66] H. Wang, F. Shadman, Effect of particle size on the adsorption and desorption properties of oxide nanoparticles, AIChE J. 59 (2012) 1502–1510, https://doi.org/10.1002/aic.13936.
[67] H. Wang, L. Zhang, Z. Chen, J. Hu, S. Li, Z. Wang, J. Liu, X. Wang, Semiconductor heterojunction photocatalysts: Design, construction, and photocatalytic performances, Chem. Soc. Rev. 43 (2014) 5234–5244, https://doi.org/10.1039/c4cs00126e.
[68] W.K. Jo, T.S. Natarajan, Influence of TiO_2 morphology on the photocatalytic efficiency of direct Z-scheme g-C_3N_4/TiO_2 photocatalysts for isoniazid degradation, Chem. Eng. J. 281 (2015) 549–565, https://doi.org/10.1016/j.cej.2015.06.120.
[69] S. Hariganesh, S. Vadivel, D. Maruthamani, M. Kumaravel, B. Paul, N. Balasubramanian, T. Vijayaraghavan, Facile large scale synthesis of $CuCr_2O_4$/

CuO nanocomposite using MOF route for photocatalytic degradation of methylene blue and tetracycline under visible light, Appl. Organomet. Chem. 34 (2020) e5365, , https://doi.org/10.1002/aoc.5365.
[70] L. Clarizia, D. Spasiano, I. Di Somma, R. Marotta, R. Andreozzi, D.D. Dionysiou, Copper modified-TiO_2 catalysts for hydrogen generation through photoreforming of organics. A short review, Int. J. Hydrogen Energy. 39 (2014) 16812–16831, https://doi.org/10.1016/j.ijhydene.2014.08.037.
[71] J. Yu, Y. Hai, M. Jaroniec, Photocatalytic hydrogen production over CuO-modified titania, J. Colloid Interface Sci. 357 (2011) 223–228, https://doi.org/10.1016/j.jcis.2011.01.101.
[72] A. Kubiak, K. Siwińska-Ciesielczyk, J. Goscianska, A. Dobrowolska, E. Gabała, K. Czaczyk, T. Jesionowski, Hydrothermal-assisted synthesis of highly crystalline titania–copper oxide binary systems with enhanced antibacterial properties, Mater. Sci. Eng. C. 104 (2019), https://doi.org/10.1016/j.msec.2019.109839.
[73] P. Wang, P.S. Yap, T.T. Lim, C-N-S tridoped TiO_2 for photocatalytic degradation of tetracycline under visible-light irradiation, Appl. Catal. A Gen. 399 (2011) 252–261, https://doi.org/10.1016/j.apcata.2011.04.008.
[74] M. Ahmadi, H. Ramezani Motlagh, N. Jaafarzadeh, A. Mostoufi, R. Saeedi, G. Barzegar, S. Jorfi, Enhanced photocatalytic degradation of tetracycline and real pharmaceutical wastewater using MWCNT/TiO_2 nano-composite, J. Environ. Manage. 186 (2017) 55–63, https://doi.org/10.1016/j.jenvman.2016.09.088.
[75] X.D. Zhu, Y.J. Wang, R.J. Sun, D.M. Zhou, Photocatalytic degradation of tetracycline in aqueous solution by nanosized TiO_2, Chemosphere 92 (2013) 925–932, https://doi.org/10.1016/j.chemosphere.2013.02.066.
[76] Y. Shi, Z. Yang, B. Wang, H. An, Z. Chen, H. Cui, Adsorption and photocatalytic degradation of tetracycline hydrochloride using a palygorskite-supported Cu_2O-TiO_2 composite, Appl. Clay Sci. 119 (2016) 311–320, https://doi.org/10.1016/j.clay.2015.10.033.
[77] R.A. Palominos, M.A. Mondaca, A. Giraldo, G. Peñuela, M. Pérez-Moya, H.D. Mansilla, Photocatalytic oxidation of the antibiotic tetracycline on TiO_2 and ZnO suspensions, Catal. Today. 144 (2009) 100–105, https://doi.org/10.1016/j.cattod.2008.12.031.
[78] G. Zhang, W. Guan, H. Shen, X. Zhang, W. Fan, C. Lu, H. Bai, L. Xiao, W. Gu, W. Shi, Organic additives-free hydrothermal synthesis and visible-light-driven photodegradation of tetracycline of WO_3 nanosheets, Ind. Eng. Chem. Res. 53 (2014) 5443–5450, https://doi.org/10.1021/ie4036687.
[79] W. Li, H. Ding, H. Ji, W. Dai, J. Guo, G. Du, Photocatalytic degradation of tetracycline hydrochloride via a CdS-TiO_2 heterostructure composite under visible light irradiation, Nanomaterials 8 (2018) 415, https://doi.org/10.3390/nano8060415.
[80] F. Chen, Q. Yang, J. Sun, F. Yao, S. Wang, Y. Wang, X. Wang, X. Li, C. Niu, D. Wang, G. Zeng, Enhanced photocatalytic degradation of tetracycline by AgI/$BiVO_4$ heterojunction under visible-light irradiation: mineralization efficiency and mechanism, ACS Appl. Mater. Interfaces 8 (2016) 32887–32900, https://doi.org/10.1021/acsami.6b12278.
[81] L. Wang, C. Zhang, R. Cheng, J. Ali, Z. Wang, G. Mailhot, G. Pan, Microcystis aeruginosa synergistically facilitate the photocatalytic degradation of tetracycline hydrochloride and Cr(VI) on PAN/TiO_2/Ag nanofiber mats, Catalysts 8 (2018) 628, https://doi.org/10.3390/catal8120628.
[82] S.J.A. Moniz, J. Tang, Charge transfer and photocatalytic activity in CuO/TiO_2 nanoparticle heterojunctions synthesised through a rapid, one-pot, microwave solvothermal route, ChemCatChem 7 (2015) 1659–1667, https://doi.org/10.1002/cctc.201500315.
[83] M. Buchalska, M. Kobielusz, A. Matuszek, M. Pacia, S. Wojtyła, W. Macyk, On oxygen activation at rutile- and anatase-TiO_2, ACS Catal. 5 (2015) 7424–7431, https://doi.org/10.1021/acscatal.5b01562.
[84] W.R. Siah, H.O. Lintang, M. Shamsuddin, H. Yoshida, L. Yuliati, Masking effect of copper oxides photodeposited on titanium dioxide: Exploring UV, visible, and solar light activity, Catal. Sci. Technol. 6 (2016) 5079–5087, https://doi.org/10.1039/c6cy00074f.
[85] B. Ohtani, Photocatalysis A to Z-What we know and what we do not know in a scientific sense, J. Photochem. Photobiol. C Photochem. Rev. 11 (2010) 157–178, https://doi.org/10.1016/j.jphotochemrev.2011.02.001.
[86] F. Amano, O.O. Prieto-Mahaney, Y. Terada, T. Yasumoto, T. Shibayama, B. Ohtani, Decahedral single-crystalline particles of anatase titanium(IV) oxide with high photocatalytic activity, Chem. Mater. 21 (2009) 2601–2603, https://doi.org/10.1021/cm9004344.
[87] S.W. Verbruggen, TiO_2 photocatalysis for the degradation of pollutants in gas phase: From morphological design to plasmonic enhancement, J. Photochem. Photobiol. C Photochem. Rev. 24 (2015) 64–82, https://doi.org/10.1016/j.jphotochemrev.2015.07.001.
[88] Z.W. Kunlei Wang, M. Janczarek, Z. Wei, T. Raja-Mogan, M. Endo-Kimura, T.M. Khedr, B. Ohtani, E. Kowalska, Morphology- and crystalline composition-governed activity of titania-based photocatalysts: overview and perspective, Catalysts 1054 (2019), https://doi.org/10.3390/catal9121054.
[89] O. Ola, M.M. Maroto-Valer, Review of material design and reactor engineering on TiO_2 photocatalysis for CO_2 reduction, J. Photochem. Photobiol. C Photochem. Rev. 24 (2015) 16–42, https://doi.org/10.1016/j.jphotochemrev.2015.06.001.
[90] M. Rokhmat, E. Wibowo, Khairurrijal Sutisna, M. Abdullah, Performance improvement of TiO_2/CuO solar cell by growing copper particle using fix current electroplating method, Proc. Eng. 170 (2017) 72–77, https://doi.org/10.1016/j.proeng.2017.03.014.
[91] A.L. Luna, M.A. Valenzuela, C. Colbeau-Justin, P. Vázquez, J.L. Rodriguez, J.R. Avendaño, S. Alfaro, S. Tirado, A. Garduño, J.M. De La Rosa, Photocatalytic degradation of gallic acid over CuO-TiO_2 composites under UV/Vis LEDs irradiation, Appl. Catal. A Gen. 521 (2016) 140–148, https://doi.org/10.1016/j.apcata.2015.10.044.
[92] S. Chu, X. Zheng, F. Kong, G. Wu, L. Luo, Y. Guo, H. Liu, Y. Wang, H. Yu, Z. Zou, Architecture of Cu_2O@TiO_2 core-shell heterojunction and photodegradation for 4-nitrophenol under simulated sunlight irradiation, Mater. Chem. Phys. 129 (2011) 1184–1188, https://doi.org/10.1016/j.matchemphys.2011.06.004.
[93] F.Y. Chen, X. Zhang, Y. Bin Tang, X.G. Wang, K.K. Shu, Facile and rapid synthesis of a novel spindle-like heterojunction BiVO4 showing enhanced visible-light-driven photoactivity, RSC Adv. 10 (2020) 5234–5240. doi: 10.1039/c9ra07891f.
[94] G. Mano, S. Harinee, S. Sridhar, M. Ashok, A. Viswanathan, Microwave assisted synthesis of ZnO-PbS heterojuction for degradation of organic pollutants under visible light, Sci. Rep. 10 (2020) 1–14, https://doi.org/10.1038/s41598-020-59066-4.
[95] M. Oghbaei, O. Mirzaee, Microwave versus conventional sintering: A review of fundamentals, advantages and applications, J. Alloys Compd. 494 (2010) 175–189, https://doi.org/10.1016/j.jallcom.2010.01.068.
[96] B.A. Roberts, C.R. Strauss, Toward rapid, “green”, predictable microwave-assisted synthesis, Acc. Chem. Res. 38 (2005) 653–661, https://doi.org/10.1021/ar040278m.
[97] S. Li, J. Hu, Photolytic and photocatalytic degradation of tetracycline: Effect of humic acid on degradation kinetics and mechanisms, J. Hazard. Mater. 318 (2016) 134–144, https://doi.org/10.1016/j.jhazmat.2016.05.100.
[98] Y. Deng, L. Tang, G. Zeng, J. Wang, Y. Zhou, J. Wang, J. Tang, L. Wang, C. Feng, Facile fabrication of mediator-free Z-scheme photocatalyst of phosphorous-doped ultrathin graphitic carbon nitride nanosheets and bismuth vanadate composites with enhanced tetracycline degradation under visible light, J. Colloid Interface Sci. 509 (2018) 219–234, https://doi.org/10.1016/j.jcis.2017.09.016.